648–665 *Nucleic Acids Research, 2011, Vol. 39, No. 2* *Published online 26 August 2010*
doi:10.1093/nar/gkq758

The NIP7 protein is required for accurate pre-rRNA processing in human cells

Luis G. Morello[1], Cédric Hesling[1,2], Patrícia P. Coltri[1,3], Beatriz A. Castilho[3], Ruth Rimokh[2] and Nilson I. T. Zanchin[1,*]

[1]Laboratório Nacional de Biociências, Centro Nacional de Pesquisa em Energia e Materiais, Rua Giuseppe Maximo Scolfaro 10000, CEP13083-970, Campinas SP, Brazil, [2]Institut National de la Santé et de la Recherche Médicale U590, Centre Léon Bérard, Université de Lyon, 69373 Lyon Cedex 08, France and [3]Department of Microbiology, Immunology and Parasitology, Universidade Federal de São Paulo, Rua Botucatu 862, São Paulo, SP 04023-062, Brazil

Received November 15, 2009; Revised August 6, 2010; Accepted August 9, 2010

ABSTRACT

Eukaryotic ribosome biogenesis requires the function of a large number of *trans*-acting factors which interact transiently with the nascent pre-rRNA and dissociate as the ribosomal subunits proceed to maturation and export to the cytoplasm. Loss-of-function mutations in human *trans*-acting factors or ribosome components may lead to genetic syndromes. In a previous study, we have shown association between the SBDS (Shwachman–Bodian–Diamond syndrome) and NIP7 proteins and that downregulation of SBDS in HEK293 affects gene expression at the transcriptional and translational levels. In this study, we show that downregulation of NIP7 affects pre-rRNA processing, causing an imbalance of the 40S/60S subunit ratio. We also identified defects at the pre-rRNA processing level with a decrease of the 34S pre-rRNA concentration and an increase of the 26S and 21S pre-rRNA concentrations, indicating that processing at site 2 is particularly slower in NIP7-depleted cells and showing that NIP7 is required for maturation of the 18S rRNA. The NIP7 protein is restricted to the nuclear compartment and co-sediments with complexes with molecular masses in the range of 40S–80S, suggesting an association to nucleolar pre-ribosomal particles. Downregulation of NIP7 affects cell proliferation, consistently with an important role for NIP7 in rRNA biosynthesis in human cells.

INTRODUCTION

Biogenesis of eukaryotic ribosomes involves synthesis and assembly of four ribosomal RNAs (rRNA) with about 80 ribosomal proteins mediated by more than 170 *trans*-acting factors. A significant amount of the cell energy is devoted to the maturation of three of the four eukaryotic rRNA molecules (18S, 5.8S and 25/28S) which are generated from a single transcript containing the sequences of the mature rRNAs flanked by spacer sequences. During rRNA maturation, the spacer sequences are excised by a series of endo and exonucleolytic cleavages and, at specific positions defined by sequence complementarity to snoRNAs, bases or riboses are modified by methylation and uridines are converted to pseudouridines (1–4). The pre-rRNA processing pathway is best characterized in the *Saccharomyces cerevisiae* model system. In wild-type strains, pre-rRNA maturation follows a 5′ to 3′ processing hierarchy where the 5′ ETS (external transcribed spacer sequence) is cleaved before processing in ITS1 (internal transcribed spacer sequence 1), which in its turn is cleaved before ITS2 (5–7).

Most of the yeast ribosome biogenesis factors have counterparts in higher eukaryotes, although not all the data obtained from the yeast system can be transferred to vertebrates. For instance, pre-rRNA maturation does not follow the 5′ to 3′ processing hierarchy in vertebrates. Instead, the order of processing depends on the species, cell type and physiological state. The mammalian pre-rRNA can be processed by simultaneous alternative pathways (8,9), following an initial cleavage that takes place at the site A′ of the 47S pre-rRNA generating the 45S pre-rRNA. The three major pathways differ in the place of the first processing step in the 45S pre-rRNA. In pathway A, the first cleavage takes place at Site 1, in

*To whom correspondence should be addressed. Tel: +55 19 3521 1144; Fax: +55 19 3521 1089; Email: zanchin@cbmeg.unicamp.br

The authors wish it to be known that, in their opinion, the first two authors should be regarded as joint First Authors.

pathway B, at Site 2c and, in pathway C, at Site 4b (Figure 1). The pathway has continuously been reviewed and novel intermediates and a cleavage site in the 5′-ETS have recently been described for mouse and human cells (10,11).

Expression of genes encoding ribosome biogenesis factors (termed Ribi regulon) is tightly regulated, showing a coordinated response to nutrient supply, physiological conditions or genetic perturbations (12–15). Transcription of this group of genes requires concerted action of the three RNA polymerases which in animals is mediated by the transcription factor Myc (16–19). Synchronized expression of the Ribi regulon involves also feedback regulation by several ribosomal proteins (20–22). Accurate synthesis of ribosomes is critical to all cells. Mutations in *S. cerevisiae* genes required for ribosome biogenesis usually interfere with the order of pre-rRNA processing steps, causing accumulation of aberrant pre-rRNAs or fast degradation of pre-rRNA intermediates. Pre-rRNA processing defects can also lead to imbalance of the 40S/60S subunit ratio or affect subunit export to the cytoplasm. In humans, mutations causing loss of function in genes encoding structural proteins or ribosome biogenesis factors may lead to genetic syndromes. Currently, there are five known syndromes associated with mutations in such genes. A series of mutations in genes encoding both 40S subunit (23–25) and 60S subunit proteins (26–28) have been linked to the

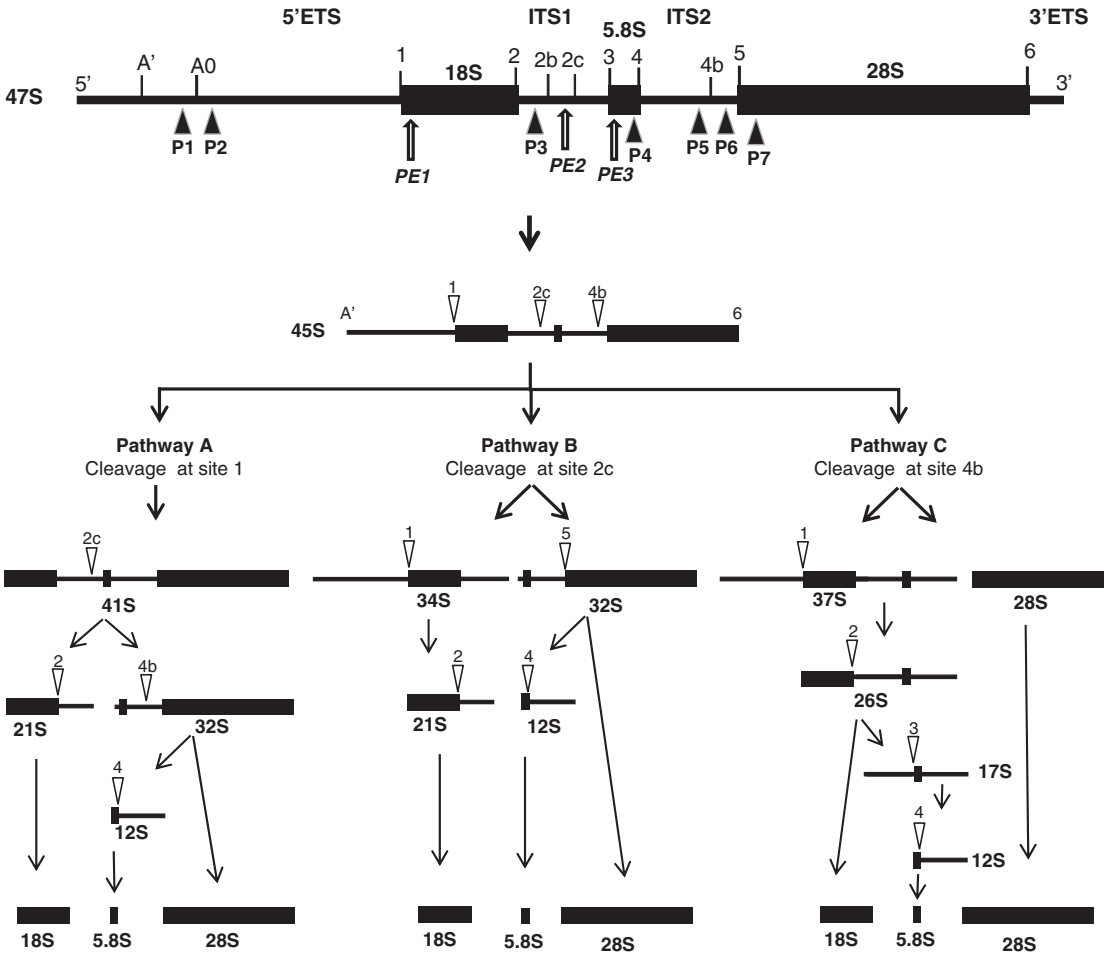

Figure 1. Schematic representation of the human pre-rRNA processing pathways. The 47S pre-rRNA is converted to the 45S pre-rRNA following the initial cleavages at sites A′ in the 5′-ETS and at site 6, at the 3′-end of the mature 28S rRNA. The 45S is processed by three alternative pathways. In pathway A, the first cleavage in 45S takes place at site 1, generating the 41S pre-rRNA whose 5′-end corresponds to the 5′-end of the mature 18S rRNA. The 41S pre-rRNA is subsequently processed at site 2c, separating the 21S pre-rRNA, from the 32S pre-rRNA. The 3′-end of the 21S pre-rRNA is processed to generate the 18S rRNA. The 32S pre-rRNA is cleaved at site 4b, generating the 12S pre-rRNA and the 28S rRNA. Finally, the 3′-end of the 12S pre-rRNA is processed to generate the mature 5.8S rRNA. In pathway B, the first cleavage in 45S takes place at site 2c, generating the 34S and 32S pre-rRNAs. The 34S pre-rRNA is subsequently processed at site 1, generating the 21S pre-rRNA. The 3′-end of the 21S pre-rRNA is processed further to generate the 18S rRNA. The 32S pre-rRNA is processed as described for pathway A. In pathway C, the first cleavage in 45S takes place at site 4b, generating the 37S and the 28S rRNA. The 37S pre-rRNA is subsequently processed at site 1, generating the 26S pre-rRNA, which is subsequently cleaved at site 2 generating the 18S rRNA and the 17S pre-rRNA. This pre-rRNA is processed at site 3 generating the 12S pre-rRNA and the 3′-end of the 12S pre-rRNA is processed to generate the mature 5.8S rRNA. This representation of the pathways was based on the papers published by Bowman *et al.* (8) and Hadjiolova *et al.* (9). Open arrowheads indicate the subsequent cleavage sites. Dark arrowheads (P1–P7) underneath the 47S pre-rRNA indicate the positions of the oligonucleotide probes used in northern blot and the open arrows (PE1–PE3) indicate the oligonucleotide probes used in primer extensions analyses, respectively.

Diamond Blackfan Anemia (DBA). In addition, Dyskeratosis Congenita has been associated with mutations in the X-linked DKC1 gene (29), encoding dyskerin, the pseudouridine synthase component of box H/ACA snoRNP. Deficiency in dyskerin abrogates pseudouridylation of rRNA and affects translation initiation of mRNAs containing internal ribosomal entry sites (IRES) (30,31). Mutations in the RNA component of the RNase MRP have been linked to Cartilage–Hair hypoplasia (CHH) (32). Mutations in the gene encoding the protein treacle are linked to the Treacher Collins syndrome. Treacle interacts with RNA polymerase I and Nop56, a subunit of the box CD snoRNP, and is involved in rRNA methylation (33,34). The Shwachman-Bodian-Diamond syndrome (SDS) is associated to mutations in the SBDS gene (35). Studies using both yeast and human cells have shown that SBDS orthologs are involved in ribosome biosynthesis and function (36–38). Dysregulation of ribosome biosynthesis and translational capacity has also been associated to pathological conditions such as human breast cancer (39).

The *S. cerevisiae* NIP7 protein is required for pre-rRNA processing and ribosome biosynthesis (40). NIP7 orthologs are highly conserved, ranging from 160 to 180 amino-acid residues and sharing a two-domain architecture with the C-terminal region corresponding to the PUA domain (named after pseudouridine synthases and archaeosine-specific transglycosylases) with a predicted RNA-interaction activity (41) that in the case of the *Pyrococcus abyssi* and *S. cerevisiae* NIP7 orthologs was already confirmed (42). The human NIP7 interacts with Nop132 (43), the putative ortholog of the *S. cerevisiae* Nop8p that is also involved in ribosome biogenesis (44). Furthermore, the human NIP7 was found in complexes isolated by affinity-tagged purification of RPS19 (45), a component of the 40S subunit that plays an essential role in its synthesis (23), and of parvulin (Par14), a peptidyl-prolyl *cis–trans* isomerase (PPIase) required for pre-rRNA processing (46). In a previous work, we have detected the interaction of NIP7 with SBDS in the yeast two-hybrid system (47). In addition, an immobilized GST–SBDS fusion protein was able to pull-down NIP7 from HEK293 cell extracts, indicating that both proteins can be part of a multisubunit complex (47).

Although the evidence above points to a role for the human NIP7 protein in ribosome biosynthesis, so far there is no report on the functional analysis of this protein. In this work, we used RNA interference to downregulate NIP7 and investigate its function in human cell lineages. We show that downregulation of NIP7 affects cell proliferation and causes imbalance of the 40S/60S subunit ratio. We also identified defects at the pre-rRNA processing level with a decrease of the 34S pre-rRNA concentration and an increase of the 26S and 21S pre-rRNA concentrations, suggesting that processing at site 2 is particularly slower in NIP7-depleted cells. The results presented in this work suggest that NIP7 is required for accurate processing of the pre-rRNAs leading to 18S rRNA maturation and 40S subunit biogenesis. At least part of the pre-rRNA processing defects caused by NIP7 downregulation have been described for other situations in which ribosome biogenesis was impaired, such as treatment with leptomycin B, which inhibits exportin Crm1/Xpo1 and blocks ribosome subunit export from the nucleus, and for downregulation of 40S biogenesis factors (11). The NIP7 protein is restricted to the nuclear compartment and co-sediments with complexes with molecular masses in the range of 40S–80S suggesting an association to nucleolar pre-ribosomal particles. This work shows that NIP7 plays a critical role in pre-rRNA maturation in human cells.

MATERIALS AND METHODS

Plasmid construction

DNA cloning was performed using the *Escherichia coli* strain DH5α which was maintained in LB medium containing $50\,mg\,ml^{-1}$ of the required antibiotic used in transformant selection and manipulated according to standard techniques (48). The *NIP7* 540-bp coding sequence was isolated from pTL1-HSNIP7 (47) using the EcoRI/SalI restriction sites and inserted into the pET28a plasmid, generating pET28-HSNIP7. The *NIP7* shRNA target was 21-residue oligonucleotide whose sequence was selected based on the Ambion siRNA Target Finder. The sequences of the oligonucleotides NIP7-shRNA-F and NIP7-shRNA-R used to generate the shRNA against the *NIP7* mRNA and of the oligonucleotides scrambled shRNA-F and scrambled shRNA-R to generate the control scrambled shRNA, scRNA, is given in Table 1. The annealed oligonucleotides were cloned into pMaleficent (49) previously digested with Esp3I/EcoRI, generating pMaleficent-shRNA-HSNIP7 and pMaleficent-scRNA-HSNIP7, respectively.

Cell culture methods and RNA interference strategies

HEK293 cells (ATCC number CRL-1573) were maintained in MEM (Minimum Essential Alfa Medium, Gibco-BRL) supplemented with 10% fetal bovine serum, $100\,U.ml^{-1}$ penicillin and $100\,\mu g.ml^{-1}$ streptomycin. The cells were cultured at 37°C in a humidified atmosphere with 5% CO_2. To generate permanent cells with downregulation of *NIP7*, we employed a mammalian transposon system designated pMaleficent/pCMVHSB#17 (49). HEK293 transfections were performed by electroporation as described by Klan and Steinhilber (50). Following transfection, HEK293 cells were transferred into six-well plates and kept under geneticin selection ($700\,\mu g.ml^{-1}$). Proliferation rates of HEK293 derivative cells were determined using the MTT {[3-(4,5-dimethylthiazolyl-2)-2,5-diphenytetrazolium bromide], Sigma} cell proliferation assay as previously described (47). Downregulation of NIP7 in HeLa and MCF10A cells was achieved by using transient transfections of siRNA. For each assay, 1.5×10^5 cells (~60–80%confluence) were harvested in OPTI MEM (Invitrogen) and transfected with 5 or 10 nM siRNA oligonucleotides (NIP7-siRNA-F and NIP7-siRNA-R, Table 1) using 0.5 µl/ml lipofectamine RNAiMax Transfection Reagent (Invitrogen) following the

Table 1. Primers used in this study

Primer name	Sequence
NIP7-shRNA-F	5′ TCC CGA ACC ATG TGT TGA AAT CTG GTT TCA AGA GAA CCA GAT TTC AAC ACA TGG TTC TTT TTT G 3′
NIP7-shRNA-R	5′ AAT TCA AAA AAG AAC CAT GTG TTG AAA TCT GGT TCT CTT GAA ACC AGA TTC AAC ACA TGG TTC 3′
Scrambled shRNA-F	5′ TCC CGA ATT TGT GAT CCA GGA ATG CTT TCA AGA GAA GCA TTC CTG GAT CAC AAA TTC TTT TTT G 3′
Scrambled shRNA-R	5′ AAT TCA AAA AAG AAT TTG TGA TCC AGG AAT GCT TCT CTT GAA AGC ATT CCT GGA TCA CAA ATT C 3′
NIP7-siRNA-F	5′ GCA CCU ACU GUU UCC GUC UGC ACA A 3′
NIP7-siRNA-R	5′ UUG UGC AGA CGG AAA CAG UAG GUG C 3′
Actin-F	5′ TGG ATC AGC AAG CAG GAG TAT G 3′
Actin-R	5′ GCA TTT GCG GTG GAC GAT 3′
NIP7-F	5′ CCG GGT GTA CTA TGT GAG TGA GAA 3′
NIP7-R	5′ TTG TGG GTT TTA GTG AAT TTT CCA 3′
HPRT-F	5′ TGA CCT TGA TTT ATT TTG CAT ACC 3′
HPRT-R	5′ CGA GCA AGA CGT TCA GTC CT 3′
36B4-F	5′ GTG TTC GAC AAT GGC AGC AT 3′
36B4-R	5′ GAC ACC CTC CAG GAA GCG A 3′
P1	5′ CCC CAA GGC ACG CCT CTC AGA TCG CTA GAG AAG GCT TTT C 3′
P2	5′ CCA CGC AAA CGC GGT CGT CGG CAC CGG TCA CGA CTC GGC A 3′
P3	5′ AAG GGG TCT TTA AAC CTC CGC GCC GGA ACG CGC TAG GTA C 3′
P4	5′ GCG TTC GAA GTG TCG ATG ATC AAT GTG TCC TGC AAT TCA C 3′
P5	5′ CGG GAA CTC GGC CCG AGC CGG CTC TCT CTT TCC CTC TCC G 3′
P6	5′ GGG GAG AGG CGA CGG GAG AGA GAG CGC 3′
P7	5′ CTT TTC CTC CGC TGA CTA ATA TGC TTA 3
PE1	5′ GAC ATG CAT GGC TTA ATC TTT GAG ACA AGC 3′
PE2	5′ GTA AAG CCC CCA CCC GAC GGC CGC CG 3′
PE3	5′ CTC GCA GCT AGC TGC GTT CTT CAT CGA C 3′
MM21	5′ CAC AAG CCC ATT TGA CAC TGA 3′
MM30	5′ CGG AAT TCC GTG GGC CTA AGT CAG ATG ATG 3′
MM36	5′ CTC GAG TTA TTC ATC AAA AAT TTG GAT TGG TAT TTC 3′
MM44	5′ CTG CAG CTC GAG TTA CCT TCG TGT ATA TTC TTC TGA TTT TTA TG 3′
MM54	5′ CTC GAG TCA ACT TTC AAG TAC AGA TGG AGC CAC ATA TTC AAA ACC CAG AAA GAC 3′
MM64	5′ AAT TCA AAA AAG AAT TTG TGA TCC AGG AAT GCT TCT CTT GAA AGC ATT CCT GGA TCA CAA ATT C 3′
MM74	5′ TCC CGT ATA ATC TGT TGT ATA GGT CCT TGA TAT CCG GGA CCT ATA CAA CAG ATT ATA TTT TTT CCA ATT TTT TG 3′

manufacturer's instructions. Parallel control transfection assays were performed with scrambled 'AllStars Negative Control siRNA' (Qiagen); Cells were plated and cultured for 12 h in antibiotic free medium. Medium was changed and cells cultured for 36–96 h in complete fresh medium. For proliferation analysis of transfected HeLa and MCF10A cells, triplicates at a density of 1500 cells/well were seeded in 96-wells plates (100 µl/well) and cultured for 4 h in complete medium. At each time point, cells were treated with 10 µl Uptiblue (Interchim) and incubated for 4 h at 37°C. Luminescent quantification was performed using a spectrophotometer (Cytofluor), excitation 590/25 nm; emission 530/25 nm. Background was measured from wells without cells and subtracted from the 530 nm values. Cell-cycle analyses were performed by fluorescence-activated cell sorting (FACS). For these assays, 0.5×10^6 cells were fixed on ice in 70% (v/v) ethanol for 30 min, washed with PBS and the DNA content stained with 20 µg/ml propidium iodide in PBS in the presence of 1 mg/ml RNAse. Cells were analyzed on a FACSCalibur™ (BD Biosciences) equipped with a 488-nm argon laser. The fluorescence was measured through a 575/25 band pass filter. Cells doublets were removed using the FL2-Area and FL2-Width parameters. Data acquisition was performed using CellQuest software (BD Biosciences) and analysis using ModFit software (Verity Software). FACS analyses were performed with the permanent HEK293 derivative cells (SC, which express the scrambled shRNA and, CP4 cells that express the RNAi against the NIP7 mRNA) and with MCF10A cells transiently transfected with either a scrambled siRNA or a NIP7 siRNA 48 h after transfection.

Analysis of NIP7 mRNA levels

NIP7 mRNA downregulation was confirmed by RT–qPCR using oligonucleotides complementary to *NIP7* sequence (NIP7-shRNA-F and NIP7-shRNA-R). One microgram of total RNA was used for cDNA synthesis using the SuperScript II Reverse Transcriptase system (Invitrogen). The mRNA levels were quantified using the SYBR Green® reagent on a 7500 Real Time PCR system (Applied Biosystems). In the case of HEK293 derivative cells, *NIP7* mRNA levels were normalized to the amount of the actin mRNA determined using primers Actin-F and Actin-R. In the case of HeLa and MCF10A cells, *NIP7*

mRNA levels were normalized to the amount of the HPRT and 36B4 mRNAs, respectively, which were determined using primers HPRT-F and HPRT-R or 36B4-F and 36B4-R, respectively. The sequences of all primers used in this work are given in Table 1. The NIP7 protein levels were determined by immunoblotting as described below.

Sucrose gradient and cell fractionation

Polysomes profiles were analyzed on sucrose gradients as previously described (51). The cells were cultivated up to 50% confluence. Following addition of 100 μg.ml^{-1} cycloheximide, 5×10^7 cells were collected and lyzed using 500 μl of polysome buffer (PB) containing 20 mM Tris–HCl pH 7.5, 100 mM NaCl, 10 mM $MgCl_2$, 1 mM DTT, 1% v/v Triton X-100 and 100 μg.ml^{-1} cycloheximide. Extracts were clarified by centrifugation at $20\,000 \times g$ for 10 min at 4°C. Totals of 255 OD_{260} units (300 μl) were loaded onto linear sucrose gradients (15–50%) prepared in PB. Polysomes were separated by centrifugation at 40 000 rpm for 4 h at 4°C using a Beckman SW41 rotor. Gradients were fractionated by monitoring absorbance at 254 nm. Protein precipitation and removal of sucrose for immunoblot analyses was performed as follows: 150 μl of each sucrose gradient fraction were mixed with 600 μl of methanol and subsequently mixed with 150 μl of chloroform; 450 μl of water were added to the mix and centrifuged at $20\,000 \times g$ for 5 min at 4°C. The aqueous layer was discarded and the pellet washed with 650 μl of methanol, followed by centrifugation as described above. The liquid was discarded and the pellet was taken up in protein sample buffer (48) and analyzed by immunoblotting. For isolation of nuclear and cytoplasmic extracts, 2×10^7 cells were washed in ice cold PBS and harvested by centrifugation at $500 \times g$ for 5 min at 4°C. Cells were lyzed in 1 ml LSB (10 mM Tris–HCl pH 7.4, 320 mM sucrose, 2 mM $MgCl_2$, 3 mM $CsCl_2$, 0.4% NP-40, 1 mM DTT) containing a protease inhibitor cocktail (Roche) for 12 min on ice. Subsequently, the lysate was centrifuged at $800 \times g$ for 2 min at 4°C, the supernatant was collected and centrifuged at $20\,000 \times g$ for 10 min and the resulting supernatant was saved as the cytoplasmic extract. The pellet from the $800 \times g$ centrifugation, containing the nuclei, was washed once with LSB and the nuclear proteins extracted in 300 μl HSB (250 mM NaCl, 50 mM Tris–HCl pH 8.0, 5 mM EDTA pH 8.0, 0.5% NP-40) containing a protease inhibitor cocktail (Roche) and 240 U of RNaseOUT (Invitrogen). The suspension was centrifuged at $20\,000 \times g$ for 10 min at 4°C and the supernatant saved as the nuclear fraction. Totals of 10 OD_{260} units of nuclear extracts were fractionated on 15–50% sucrose gradients prepared in polysome buffer as described above. For immunoblotting, aliquots of sucrose gradient fractions were processed as described above.

Immunoblot analysis

Proteins were resolved by SDS–PAGE and transferred to PVDF membranes at 80 mA for 1 h in buffer containing 25 mM Tris–base, 200 mM glycine and 20% methanol. Subsequently, membranes were blocked for 2 h with TBST buffer (20 mM Tris–HCl pH 7.5, 150 mM NaCl, 0.05% Tween 20) containing 5% low fat milk. The blots were incubated at room temperature for 2 h with primary antibodies and for 1 h with secondary antibodies. Polyclonal antisera for the human NIP7 protein were produced in rabbits and used at a 1:5000 dilution. Rabbit polyclonal antibodies for RPS6, cytoskeletal actin and GAPDH (Bethyl Laboratories) were used at a 1:5000 dilution. Mouse monoclonal for Lamin A/C and alpha-tubulin (Santa Cruz Biotechnology) were used at a 1:300 and 1:2500 dilutions, respectively. The secondary antibodies used were horseradish peroxidase-conjugated goat anti-mouse IgG (Calbiochem) and donkey anti-rabbit IgG (GE Healthcare) both at 1:5000 dilutions. The immunoblots were developed using the ECL western blotting analysis system (GE Healthcare).

RNA analysis

Total RNA from HEK293 cells, scRNA and shRNA-NIP7 clones were isolated by Trizol extraction (Invitrogen). RNAs were fractionated by electrophoresis on 1.2% (w/v) agarose/formaldehyde gels, followed by transfer to Hybond nylon membranes (GE Healthcare). Northern blot was performed using [^{32}P]-labeled oligonucleotide probes (P1–P7) complementary to specific regions of the 47S precursor RNA and submitted to autoradiography. The position of the probes were based on the human ribosomal DNA complete repeating unit, Genebank accession number U13369 (version U13369.1, GI:555853). The positions of the probes are as follows: P1 (5′ETS), complementary to nt 1401–1442; P2 (5′ETS), complementary to nt 1786–1825; P3 (ITS1), complementary to nt 6121–6160; P4 (5.8S), complementary to nt 6690–6729; P5 (ITS2), complementary to nt to 7031–7070; P6 (ITS2), complementary to nt 7812–7838 and; P7 (28S), complementary to nt 7971–7997. Primer extension analysis was performed according to Gonzales *et al.* (52) using oligonucleotide probes PE1 (18S), complementary to nt 3685–3714, PE2 (ITS1), complementary to nt 6299–6324 and PE3 (5.8S), complementary to nt 6655–6682 (Table 1). [^{32}P]-labeled-oligonucleotides MM21, MM30, MM36, MM44, MM54, MM64 and MM74 (Table 1) were used as molecular markers corresponding to 21, 30, 36, 44, 54, 64 and 74 nt, respectively. For metabolic labeling of RNA, HEK293 cells cultured on 100-mm plates at ~70–80% confluence were pre-incubated for 30 min in phosphate-free DMEM (GIBCO) supplemented with 10% FCS. Subsequently, [^{32}P]-orthophosphate (15 μCi/ml) was added to the cultures that were incubated for 45 min and the medium was replaced by cold MEM (GIBCO) supplemented with 10% FCS. Cells were collected at time 0, 30, 60 and 120 min after changing the medium. Total RNA was extracted with Trizol (Invitrogen), and 10 μg were separated by electrophoresis on agarose/formaldehyde gels and revealed by autoradiography. RNA was extracted from sucrose gradient fractions as follows: 700 μl of each fraction were transferred to 1.5 ml tubes and 42 μl of a 10% SDS solution was added to obtain a final SDS percentage of 0.6. The suspension

was subjected to two sequential extractions, the first with 700 µl of phenol/chloroform/isoamyl alcohol (25:24:1) and the second with phenol/chloroform (1:1) and the aqueous phase was transferred to a new tube and the RNA precipitated with 700 µl of isopropanol for 1 h at −20°C. The RNA was sedimented by centrifugation (12 000 × *g* for 10 min at 4°C). The RNA pellet was washed with 75% ethanol, air dried and suspended in 10 µl of DEPC-treated water.

Electrophoretic mobility shift assays (EMSA)

For recombinant NIP7 protein production, we used plasmid pET28-HSNIP7, which was constructed by transferring the 540-bp NIP7 coding sequence from plasmid pTL1-HSNIP7 (47) to plasmid pET28a, using the EcoRI/SalI restriction sites. Expression of NIP7 was performed in *E. coli* BL21(DE3) cells transformed with vector pET28-HSNIP7 and incubated in LB medium containing kanamycin (50 µg ml^{-1}) at 25°C. At an OD_{600} of ~0.8, the culture was induced by adding 0.5 mM IPTG and incubating at 25°C for further 4 h. Cells were harvested by centrifugation, suspended in buffer containing 50 mM sodium phosphate pH 7.2, 100 mM NaCl, 10% glycerol and 0.5 mM phenylmethylsulfonyl fluoride (PMSF) and treated with lysozyme (50 µg ml^{-1}) for 30 min on ice. Subsequently, the cells were disrupted by sonication and the histidine-tagged NIP7 purified by metal-chelating affinity chromatography, using a 20–200 mM imidazole gradient for elution. NIP7 was further purified on a heparin–sepharose column using the same buffer as above for binding and a 50 mM to 1 M KCl gradient for elution. For EMSA, 20 pmol of the RNA oligoribonucleotides poly-$A_{(20)}$, poly-$U_{(20)}$ and poly-$AU_{(21)}$, (5′ UUA UUA UUU AUU UAU UAU UUA 3′) were [^{32}P]-labeled using 1 U T4 PNK and 20 µCi [γ^{32}P]-ATP. 0.4 pmol of [^{32}P]-labeled oligoribonucleotide was incubated with the indicated concentrations of NIP7 in buffer A (20 mM Tris–Cl pH 8.0, 5 mM magnesium acetate, 150 mM potassium acetate, 0.2% v/v Triton X-100, 1 mM DTT, 1 mM PMSF) for 30 min at 37°C. Complexes were resolved on 8% polyacrylamide gels using TBE buffer pH 8.0 for electrophoresis and visualized by autoradiography. RNA competition assays were performed with 1, 5 and 10 pmol of either poly-$A_{(20)}$ or poly-$AU_{(21)}$ oligonucleotides.

RESULTS

Knockdown of NIP7

The strategy to generate HEK293 cells knockdown for NIP7 was based on the generation of stably-transfected cells expressing a shRNA targeting the *NIP7* mRNA using pMaleficent as shRNA delivery vector (49). The efficiency of *NIP7* downregulation was determined by analysis of the *NIP7* mRNA and protein levels. Quantitative RT–PCR indicated that the reduction of *NIP7* mRNA levels reached up to 80% of the parental and control cells (Figure 2A). Although the levels of the NIP7 mRNA are similar in clones CP4 and CP6, the reduction in NIP7 protein levels was more efficient in clone CP4 as observed by western blot analysis (Figure 2C). Downregulation of NIP7 in these clones was stable over the period of this study. CP4 cells showed significant reduction of the proliferation rate (Figure 2E).

RNA interference based on transient transfection of siRNA oligoribonucleotides was used to downregulate NIP7 also in MCF10A and HeLa cells. The NIP7 mRNA levels were reduced to levels <10% of control cells (Figure 2B). In siRNA-treated cells, NIP7 protein was below the detection level as determined by immunoblotting. A significant reduction in the proliferation rate of both cell lines was observed following transfection with the NIP7 siRNA (Figure 2F). The reduced proliferation rate prompted us to perform fluorescence-activated cell sorting (FACS) to investigate cell-cycle progression in these cells. In the case of the permanently transfected HEK293 derivative cells, CP4 show the highest number of cells in the G0–G1 phases and the lowest number in the S phase (Table 2). This effect on the cell cycle, despite of being mild, is consistent with the results observed for MCF10A cells. NIP7 downregulation in MCF10A resulted in an increase of cells in the G0–G1 phases with an equivalent reduction of the number of cells in the S phase (Table 2). This result shows that downregulation of NIP7 lead to accumulation of cells in the G1–S transition.

Analysis of polysomes in HEK293 cells depleted of NIP7

Defects in ribosome biogenesis can in some cases be detected by using sucrose density fractionation of polysomes especially when there is an imbalance in the 40S/60S subunit ratio. The CP4 clone, showing lower NIP7 levels, was chosen for further characterization. NIP7-depleted CP4 cells showed significant reduction of 40S ribosomal subunits (Figure 3C and D). This finding is consistent with the cell proliferation assay and suggests that the reduction in growth rate is due to defective 40S subunit biosynthesis.

Analysis of pre-rRNA processing intermediates in NIP7 deficient cells

Steady-state analysis of pre-rRNA processing was assessed by northern blotting using probes complementary to the transcribed spacer sequences and to the mature rRNAs. The boundaries of most pre-rRNAs intermediates relevant to this work have already been mapped (8–11). A set of northern blots was performed with probes P1, P2, complementary to the 5′-ETS upstream and downstream of Site A0, respectively, and with probe P3 complementary to ITS1, upstream Site 2b (Figure 4). A second set of northern blots was performed with probes P4–P7 that are complementary to the 5.8S rRNA to ITS2 upstream and downstream Site 4b and to the 28S rRNA, respectively (Figure 5).

The precursors most affected are the 21S, 26S/A0-2c and 34S with the 21S and 26S/A0-2c pre-rRNAs showing increased levels and the 34S pre-rRNA showing reduced levels in NIP7 deficient cells (Figure 4). The 26S pre-rRNA running slightly faster than the mature 28S rRNA is detected with probes P2 and P3 but not by

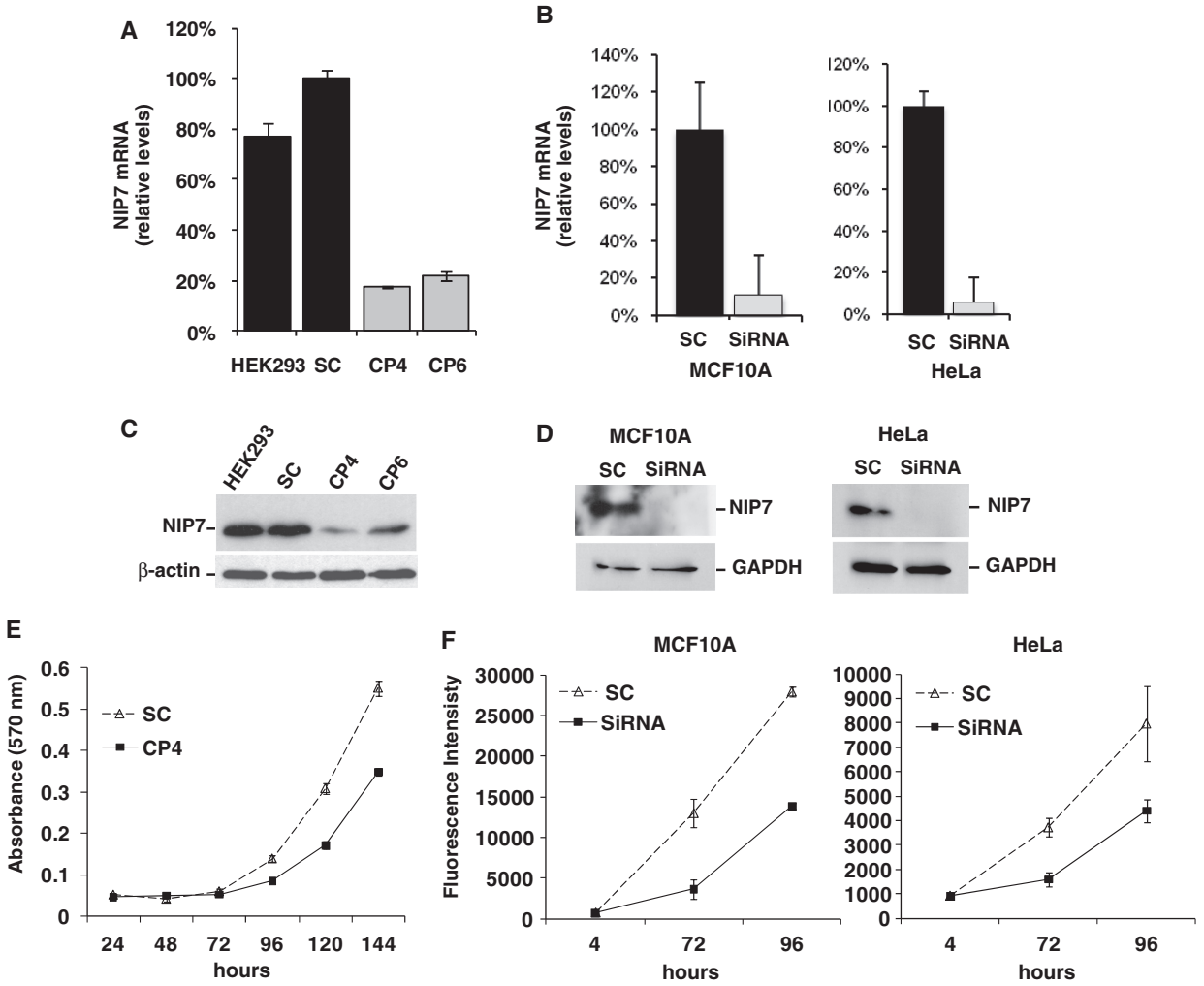

Figure 2. Analysis of NIP7 knockdown. (**A**) NIP7 mRNA levels as determined by quantitative RT–qPCR in HEK293 derivative cells. HEK293, parental cells; SC, cells transfected with a scrambled shRNA; CP4 and CP6, cells transfected with shRNA against the NIP7 mRNA. NIP7 mRNA quantitation was performed using three different RNA extractions from clones CP4 and CP6. (**B**) NIP7 mRNA levels in transiently transfected MCF10A and HeLa cells. SC, control cells transfected with scrambled RNA; SiRNA, cells transfected with siRNA against NIP7. The histogram corresponds to one of the three independent transfections of MFC10A and HeLa cells using three replicates for each cell treatment. The amount of NIP7 mRNA in cells treated with the scrambled shRNA was considered as 100% to calculate its relative levels in the parental cells (HEK293) and in cells expressing the RNAi against the NIP7 mRNA (CP4) or in cells transfected with siRNA against the NIP7 mRNA. (**C**) Immunoblot showing the levels of the NIP7 protein in HEK293 derivative cells β-actin was used as an internal control. (**D**) Immunoblot using antiserum for the NIP7 protein in transiently transfected MCF10A and HeLa cells. (**E**) Proliferation rate of HEK293 derivative cells expressing the scrambled shRNA (SC) and the RNAi against the NIP7 mRNA (CP4) over a 7-day period. (**F**) Proliferation rate of transiently transfected MCF10A and HeLa cells. The graphs correspond to one of the two independent proliferation assays performed using three replicates for each cell treatment.

Table 2. Cell-cycle distribution of NIP7-depleted cells

Cell type	Cell-cycle distribution (%)		
	G0/G1	S	G2
HEK293	49	37	14
HEK293/SC	43	42	15
HEK293/CP4	51	33	16
MCFA10A/SC	47	35	18
MCFA10A/RNAi	73	13	14

Percentage numbers represent the average of three independent experiments.

probe P1 and therefore extends from Sites A0 to 2c (Figure 4B, C and E). We concluded that this pre-rRNA corresponds to the 26S pre-rRNA described by Rouquette and co-workers (11) who defined its extension as from site A0 to a site in ITS1 downstream of nt 5687 and upstream of nt 6613, which must correspond to either Site 2b or 2c. Another precursor named 26S pre-rRNA, extending from Sites 1 to 4b, was described for pathway C [Figure 1, (8)]. However, the possibility that this pre-rRNA is increased was excluded because it was not detected by probes P4 and P5 (Figure 5). Probes P1–P3 can detect both the 34S and

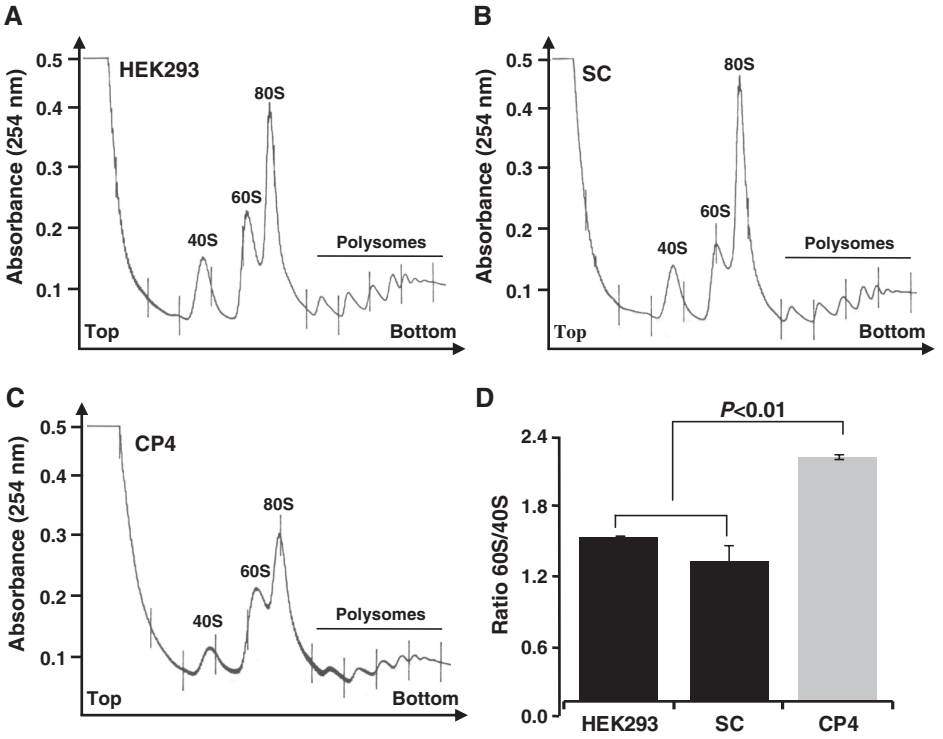

Figure 3. Analysis of polysomes by sucrose density gradient fractionation. (**A**) Polysome profile of HEK293 cells. (**B**) Polysome profile of control cells expressing the scrambled shRNA. (**C**) Polysome profiles of clone CP4 transfected with shRNA targeting the NIP7 mRNA. (**D**) Quantitation of the 60S/40S subunit ratio of HEK293 cells, control scrambled shRNA cells (SC) and of CP4 cells in the polysome profiles shown in A, B and C, respectively. CP4 cells contain a significant lower amount of 40S ribosomal subunits. *P*-value was obtained by using a one-sided Student's *t*-test ($P < 0.01$). Quantitation was based on two independent experiments performed using two replicates.

the 37S pre-rRNAs while probes P4 and P5 can detect both the 37S and the 32S pre-rRNAs (Figures 4 and 5). The 34S and 37S pre-rRNAs, comprising respectively ~6000 and ~7520 nt, may migrate with similar electrophoretic mobility in these gels. In the case of probes P1–P3 (Figure 4), a strong reduction of the signal is observed in this region of the northern blots, indicating that if any 37S pre-rRNA is generated in this cells its concentration is also decreased in NIP7-depleted cells.

A reduction in the concentration of the 32S pre-rRNA can be visually detected in the northern blots with probes P5, P6 and P7 in the NIP7 deficient cell line (Figure 5). The levels of the 41S pre-rRNA are slightly increased in NIP7 deficient cells (Figures 4C, E, 5A–C and F). This pre-rRNA, extending from sites 1 to 6, corresponds to the second largest band detected by probes P3–P6 (Figures 4C, E, 5A–C and F). The levels of the 47S and 45S pre-rRNAs, on the other hand, show a slight decrease in NIP7 deficient cells (Figures 4A–E and 5F).

Accumulation of the 26S/A0-2c pre-rRNA has been described in situations in which there is uncoupling of processing at Sites 1 and 2. Leptomycin B (LMB) inhibits exportin Crm1/Xpo1 and blocks ribosome subunit export from the nucleus. We have analyzed pre-rRNA processing of control cells (SC) and NIP7 shRNA cells (CP4) treated with LMB (Figure 4F). Upon a 4 h LMB treatment, SC cells showed a sharp increase of the 26S/A0-2c pre-rRNA. In CP4 cells, that already contain increased levels of the 26S/A0-2c and 21S pre-rRNAs, LMB treatment has a small effect on the accumulation of the 26S/A0-2c pre-rRNA. Accumulation of the 26S/A0-2c is consistent with slower processing of sites 1 and 2 in NIP7-depleted cells. However, accumulation of the 21S pre-rRNA and of the 41S pre-rRNA indicates that processing at sites 2c/2b and 2 are even slower that at site 1, suggesting that NIP7 is particularly required for processing of the ITS1 sites. Northern blot analysis with probe P3 was performed also with RNA samples from MCF10A cells (Supplementary Data), which detected accumulation of the 21S and 41S pre-rRNAs following downregulation of Nip7, indicating that Nip7 plays an important function in all cell types.

The 37S pre-rRNA (spanning from Sites A′ to 4b) and the 17S pre-rRNA (spanning from Sites 2b to 4b) would be generated only if the pathway C proposed by Bowman and co-workers (8) is indeed taking place in HEK293 cells. Gel electrophoreses used in this work resolved the 28S rRNA (5035 nt) from the 26S/A0-2c pre-rRNA (~4642 nt). Therefore, it would be expected that the 37S pre-rRNA (~7520 nt) would also be separated from the 32S pre-rRNA (6337 bases from sites 3 to 6). However, probes 4 and 5 detected only one band in this region suggesting that HEK293 cells produce low levels of the 37S pre-rRNA. The 17S pre-rRNA could be detected by probes P3, P4 and P5 (Figures 4C, 5A and B) but only

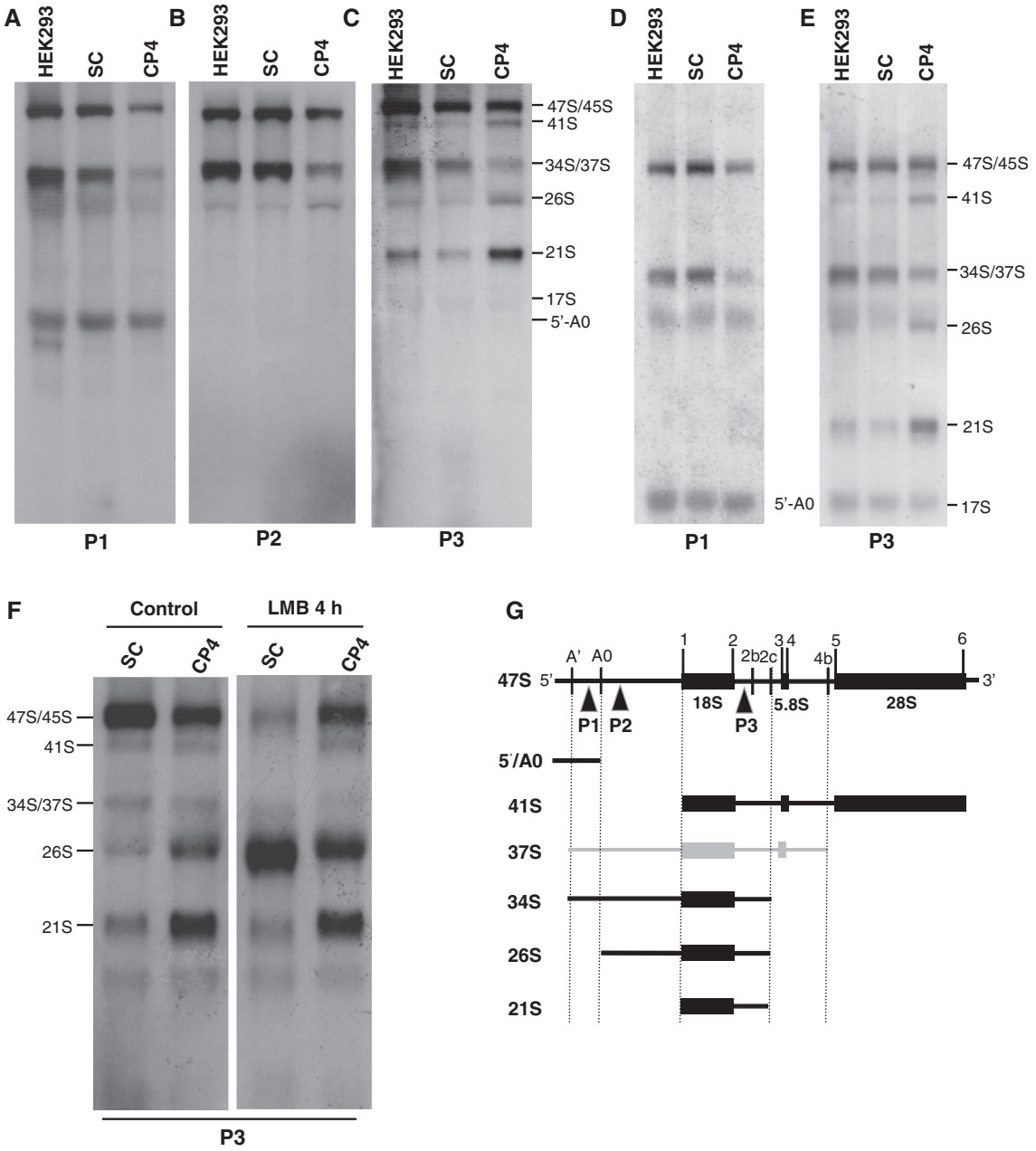

Figure 4. Northern blot analysis of pre-rRNAs detected by using probes complementary to the 5′-ETS and ITS1. (**A**) Northern blot using probe P1 complementary to the 5′-ETS upstream site A0. (**B**) Northern blot using probe P2 complementary to the 5′-ETS downstream site A0. (**C**) Northern blot using probe P3 complementary to ITS1 upstream site 2c. (**D**) and (**E**) Northern blots using probes P1 and P3 of longer electrophoresis runs. (**F**) Northern blot of cells treated with leptomycin B using probe P3 complementary to ITS1 upstream site 2c. (**G**) Structure of the 47S pre-rRNA and pre-rRNA intermediates that are most affected in NIP7-depleted cells. The positions of the probes P1, P2 and P3 used in the northern blots shown in A–D are indicated. HEK293, parental cells; SC, cells transfected with the scrambled shRNA; CP4, cells transfected with shRNA against the NIP7 mRNA.

faint bands are detected in this region. The low levels of both 17S and 37S pre-rRNAs, together with the fact that the 17S immediate upstream precursor, namely the 26S pre-rRNA extending from sites 1 to 4b, was not detected by probes P4 and P5 (Figure 5A and B) are strong indications that pathway C is a minor pathway in HEK293 cells.

An additional band with mobility similar to the 5.8S rRNA is detected with probe P5 ('Asterisk' in Figure 5B). This band might correspond to a fragment comprising from site 4b to an upstream site in ITS2 but only if there would be a cryptic endonucleolytic cleavage site downstream of site 4, which can now be speculated, following the recent discovery of the endonucleolytic activity associated to the exosome, the main *trans*-acting factor responsible for maturation of the 5.8S rRNA 3′-end (53).

Analysis of the pre-rRNA processing kinetics was performed by metabolic labeling with [^{32}P]-orthophosphate

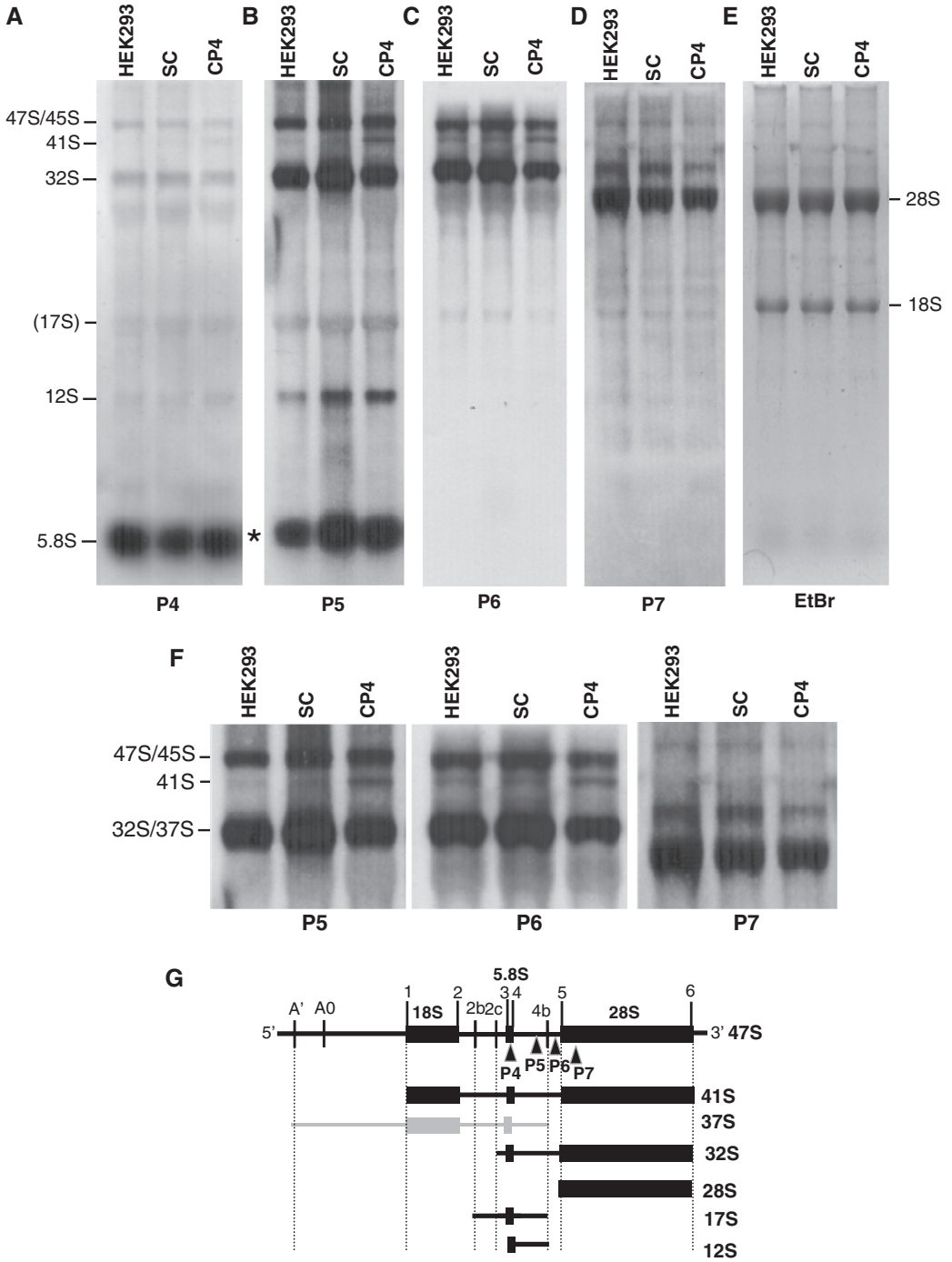

Figure 5. Northern blot analysis of pre-rRNAs detected by using probes complementary to the 5.8S rRNA, ITS2 and the 28S rRNA. (**A**) Northern blot using probe P4 complementary to the 5.8S rRNA. (**B**) Northern blot using probe P5 complementary to ITS2 upstream site 4b. (**C**) Northern blot using probe P6 complementary to ITS2 downstream site 4b. (**D**) Northern blot using probe P7 complementary to the 28S rRNA. (**E**) Ethidium bromide staining of an RNA gel showing the amounts of RNA loaded in each lane. (**F**) Enlarged figures showing the gel region of the high molecular weight pre-rRNAs detected with probes P5, P6 and P7. HEK293, parental cells; SC, cells transfected with the scrambled shRNA; CP4, cells transfected with shRNA against the NIP7 mRNA. (**G**) Structure of the 47S pre-rRNA. The positions of the probes P4, P5, P6 and P7 used in the northern blots shown in A-D are indicated. Asterisk indicates an unidentified band.

(Figure 6). By visual analysis of the autoradiograph, it is possible to observe the 21S pre-rRNA, although faint, in NIP7-depleted cells at the 2 h time point. Quantitation of the bands and calculation of the ratio relative to the amount of the 47S pre-rRNA revealed that formation of the 34S pre-rRNA is reduced and the 21S pre-rRNA is increased in NIP7-depleted cells (Figure 6B), which is consistent with the steady-state analyses, showing a defect in processing of ITS1.

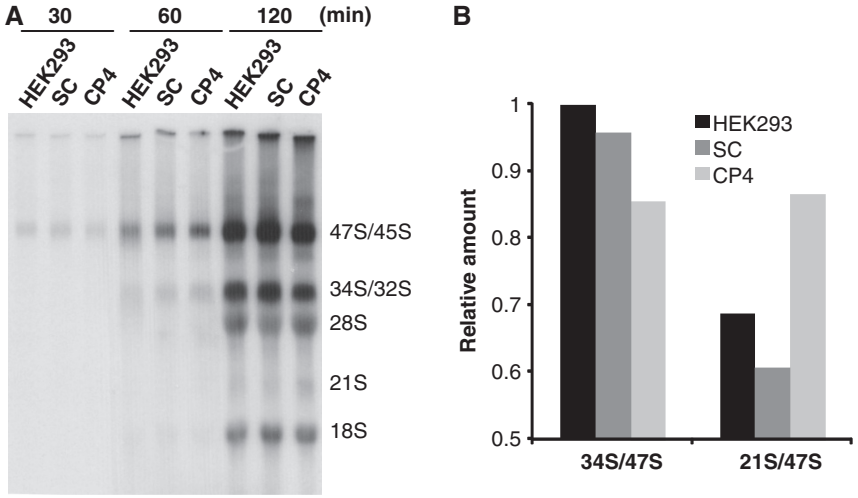

Figure 6. Analysis of pre-rRNA processing kinetics by pulse-chase labeling with ^{32}P-orthophosphate. (**A**) Autoradiography of the RNA samples that were collected every 30 min over a period of 2 h and fractionated by agarose gel electrophoresis. (**B**) Ratio of the 34S and 21S pre-rRNAs relative to the amount of the 47S pre-rRNA. Samples of the 120-min time point were used for quantitation. The 34S/47S ratio in HEK293 cells was taken as 100% to estimate the relative ratio of precursors.

Primer extension analysis of pre-rRNA processing sites in NIP7 deficient cells

Primer extension analyses were performed to examine the 5′-end of rRNA products at the processing sites that appeared to be most affected according to the northern blot analyses (Figure 7). Primer extension with oligonucleotide PE1 complementary to a sequence in the 18S rRNA, 27 bases downstream of the predicted 5′-end of the mature 18S rRNA (Site 1), resulted in products with the expected size (57, 30 nt of the primer PE1 plus 27 nt of extension up to Site 1). Interestingly, however, two bands were observed for all samples, suggesting that the cleavage at site 1 may take place at two adjacent nucleotides. For the parental HEK293 cells and the control cells transfected with the scrambled shRNA, the two bands showed a 1:1 ratio (Figure 7A). NIP7-depleted cells showed different product ratios with a sharp reduction of the longer product (Figure 7A). These discrepancies are consistent with defective processing at site 1 in NIP7-depleted cells. Oligonucleotide PE2 complementary to a sequence in ITS1 (nt 6299–6324 in the pre-rRNA) downstream of probe P3 (complementary to ITS1 nt 6121–6160 in the pre-rRNA) was used to determine the efficiency of cleavage reactions at sites in ITS1. Extension of primer PE2 generated a product of 33 nt (26 nt of the primer and 7 nt of extension), which corresponds to the 5′-end of the pre-rRNAs generated by cleavage at site 2b (Figure 7B). A reduction in the primer extension product is observed in NIP7-depleted cells, corroborating the results of the northern hybridizations which show inhibition of cleavages in ITS1 as a consequence of the reduced levels of NIP7. Oligonucleotide PE3 is complementary to a sequence 32 bases downstream of site 3, the predicted 5′-end of the mature 5.8S rRNA (nt 6655–6682 in the pre-rRNA). Extension of primer PE3 generated two major products, one with 60 nt (28 nt of the primer plus 32 nt of extension), corresponding to the expected size of the product generated by cleavage at site 3 and another one, 8–10 nt longer, designated as 3_L (Figure 7C). In eukaryotes, the 5′-end of the 5.8S rRNA has been described as heterogeneous (54–56) and this result suggests that mammalians may have at least a second form of 5.8S rRNA showing extended 5′-end as observed for *S. cerevisiae* (57). Similarly to the extension of primers PE1 and PE2, knocking down NIP7 expression caused a reduction especially of the longer extension products at site 3. The primer extension results, therefore, confirm the observation described above that lowering NIP7 expression leads to defects in pre-rRNA processing, affecting more strongly processing of the 5′-ETS and ITS1 spacer sequences.

Extension of primer PE3 revealed also three additional products (Figure 7C) that end at positions U7, U14 and A17 of the mature 5.8S rRNA (shorter form). The 5.8S rRNA is known to be methylated at residues U14 and G77, so we can assume that the faint band at the U14 position is a primer extension stop due to methylation. There is no report in the literature about nucleotide or base modification at positions A17 and U7 of the mature 5.8S rRNA. Primer extension stops can be originated when the reverse transcriptase reaches 5′-ends, base/ribose modifications or highly stable secondary structures. The band at position A17 is barely detectable in control cells and increases in NIP7-depleted cells, suggesting that it results from NIP7 deficiency (Figure 7C). In this case it is possible to speculate that the stop was due to premature degradation of the 5.8S rRNA 5′-end in the context of NIP7 deficiency where the aberrant and misprocessed precursors might be directed for degradation. In case of stop at position U7, it is present in control and test cells and is therefore caused by something that is common to the three samples which could be any of the options mentioned above.

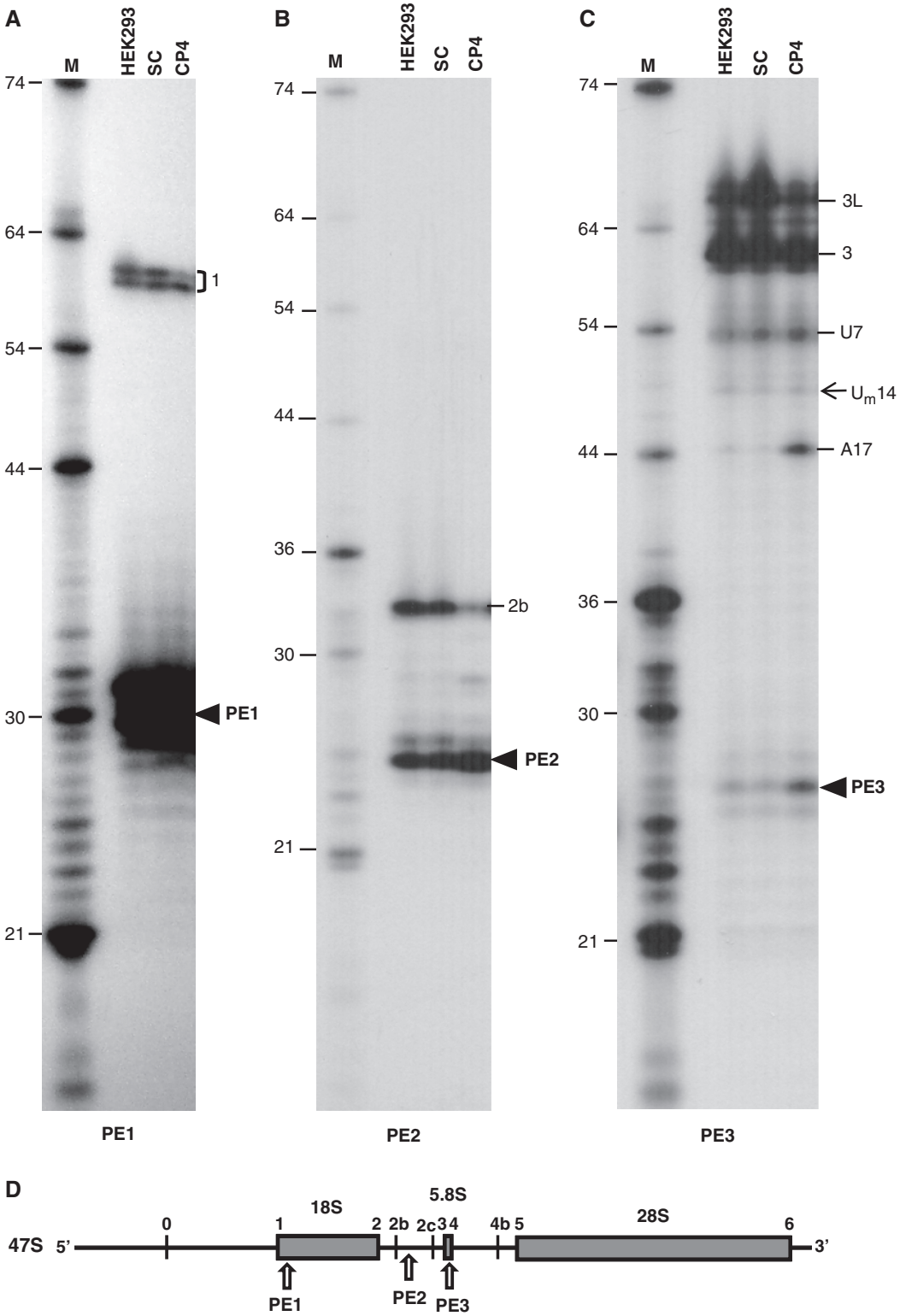

Figure 7. Analysis of primer extension products generated by reverse transcriptase. (**A**) Primer extension products using primer PE1 that is complementary to the 18S rRNA downstream site 1. (**B**) Primer extension products using primer PE2 that is complementary to ITS1 downstream site 2b. (**C**) Primer extension products using primer PE3 that is complementary to the 5.8S rRNA downstream site 3. U_m14 indicates the position of the 2-*O*-methyluridine at position 14 of the 5.8S rRNA. U7 and A17 indicate two unexpected primer extension stops. 1, 2b, 3 and 3L indicate the primer extension products extended to the respective processing sties. Arrowheads indicate the bands corresponding to the primers which were not extended: PE1, 30 nt; PE2, 26 nt and PE3, 28 nt, respectively. HEK293, parental cells; SC, cells transfected with scRNA; CP4, cells transfected with shRNA against the NIP7 mRNA. (**D**) Structure of the 47S pre-rRNA with the indication of the position of the oligonucleotides PE1, PE2 and PE3 used in the primer extension assays shown in A, B and C.

Human NIP7 associates to nuclear pre-ribosomal particles

Western blot analysis of the distribution of NIP7 in sucrose gradient fractions using the regular protocol to isolate polysomal extracts (51) revealed that NIP7 co-sediments in the range of 60S–80S ribosomes (Figure 8B). This result is similar to the distribution of *S. cerevisiae* Nip7p in sucrose gradients (40). However, previous data indicated that human NIP7 is a nucleolar protein (43). Cell fractionation followed by immunoblot analysis can be used to determine protein subcellular localization with a reasonable accuracy that, in some cases, can complement immunofluorescence assays or localization based on fusion to fluorescent proteins. Therefore, cell fractionation experiments were performed and confirmed that NIP7 is restricted to the nuclear compartment (Figure 8C). In a second experiment the sucrose gradient fractionation was performed with nuclear extract. A regular sucrose gradient with whole-cell polysomal extract was performed in parallel so that the positions of the 40S and 60S ribosomal subunits, 80S ribosomes and polysomes of the whole-cell polysomal extracts could serve as reference for sedimentation of the nuclear pre-ribosomal complexes. The fractionation analysis of the nuclear extract on sucrose gradients revealed that NIP7 distribution is highly similar to the profile observed for its distribution in the gradient of the whole-cell extract (Figure 8, compare panels B and D),

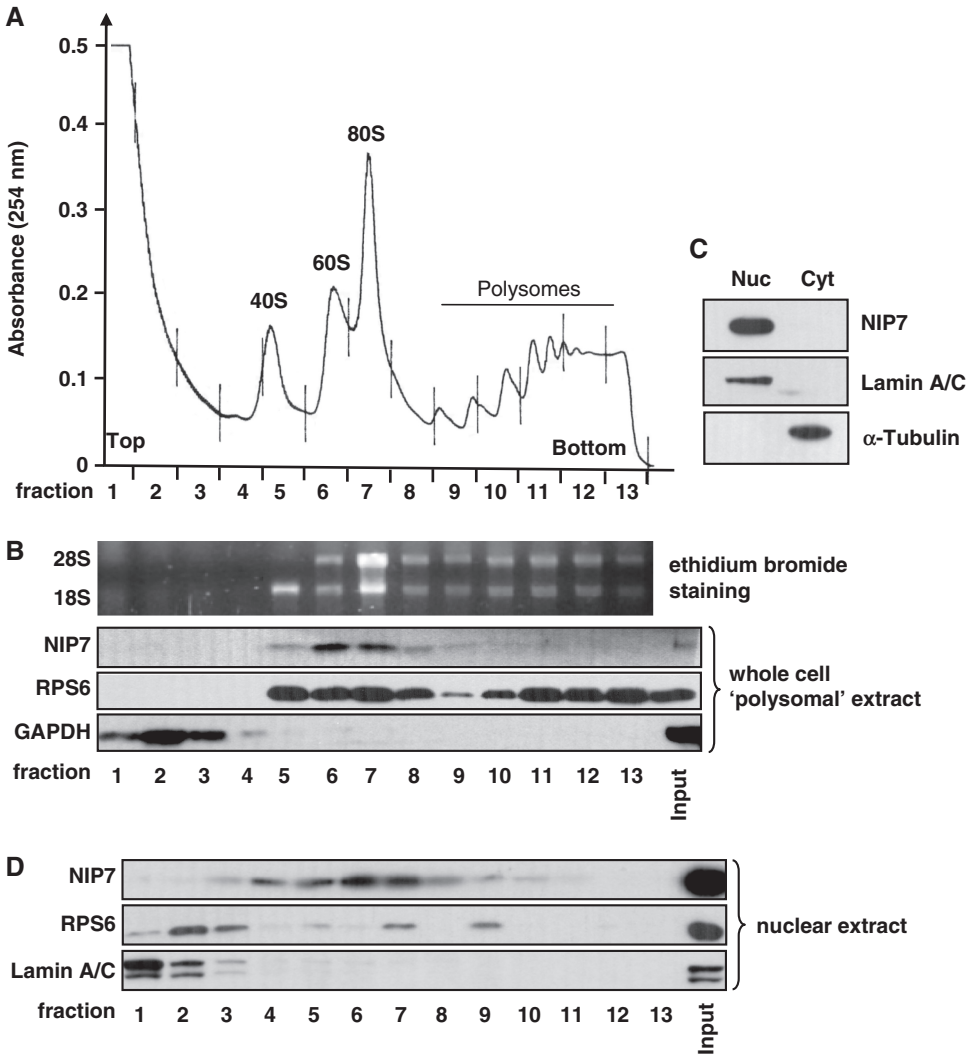

Figure 8. Analysis of NIP7 sedimentation on sucrose density gradients. (**A**) Polysome profile of HEK293 whole-cell polysomal extracts prepared according to Johannes and Sarnow (51). (**B**) Western blot analysis of NIP7 sedimentation on a sucrose density gradient of whole-cell polysomal extracts. 18S and 28S rRNAs and protein RPS6 are shown as references for ribosome and polysome sedimentation. GAPDH was used as reference for proteins not associated to ribosomes. (**C**) Western blots of HEK293 nuclear (Nuc) and cytoplasmic (Cyt) fractions showing NIP7 in the nuclear fraction. Lamin A/C and α-tubulin were used as controls for cell fractionation. (**D**) Western blot analysis of NIP7 following sucrose density gradient fractionation of a nuclear extract. The sucrose density gradients of whole-cell polysomal extract shown in B and nuclear extract shown in D were centrifuged and fractionated in parallel so that the positions of the 40S and 60S ribosomal subunits, 80S ribosomes and polysomes of the whole-cell polysomal extracts served as reference for sedimentation of the nuclear pre-ribosomal complexes. The profile of the nuclear extract is not shown because it is not informative of relevant peak fractions. RPS6 and Lamin A/C were used as references for 40S subunit and free protein sedimentation, respectively.

further suggesting that NIP7 co-sediments with pre-ribosomal particles. The control proteins used in these analyses showed the expected distribution. In the whole-cell extract gradient, RPS6 co-sediments in two major peaks, one between fractions 5 and 8, where the free 40S subunits and 80S ribosomes sediment, and between fractions 10 and 13, associated with polysomes (Figure 8B). In the gradient of nuclear extracts, on the other hand, most of RPS6, sediments in fractions 2 and 3, either as a soluble protein or as part of small complexes (Figure 8D). A smaller fraction of RPS6 sediments in fractions 5–9, indicating that it is associated to pre-ribosomal particles (Figure 8D). Lamin A/C was used as nuclear marker and behaves as a soluble protein in the sucrose gradient of the nuclear extract (Figure 8D). Consistently with the results shown above, NIP7 co-sediments with particles corresponding to pre-ribosomes in nuclear extracts gradients (Figure 8D). Combined, these results strongly indicate that NIP7 binds pre-ribosome particles in the nucleolus, thereby participating in the early pre-rRNA processing reactions.

Human NIP7 interacts with poly-U and poly-AU RNAs *in vitro*

The *S. cerevisiae* and *P. abyssi* Nip7 orthologs interact *in vitro* preferentially with poly-U homopolymers (42) and with poly-AU (J. S. Luz and C. C. Oliveira, personal communication). In order to determine whether recombinant human NIP7 also binds to RNA we initially tested its interaction with poly-U using electrophoretic mobility shift assays under native conditions. These assays showed that human NIP7 binds to polyuridine sequences although with low affinity (Figure 9A). Subsequent experiments showed that the human NIP7 protein binds to poly-AU with higher affinity than to poly-U (Figure 9B). In addition, competition assays were performed with increasing concentrations of unlabeled poly-A and poly-AU oligonucleotides. An excess of poly-A did not show effect on the NIP7–poly-AU interaction while the intensity of the band shift was reduced by increasing concentrations of unlabeled poly-AU oligonucleotides (Figure 9B and C), confirming the specificity of the NIP7–poly-AU interaction. The poly-AU oligonucleotide can form intra and intermolecular base-pairing suggesting that NIP7 might have a higher affinity for structured RNAs.

DISCUSSION

Given the essential function of the *S. cerevisiae NIP7* gene (40), the high conservation of NIP7 orthologs and the association to other ribosome synthesis proteins, we could predict that NIP7 would play an important function in human cells. We applied the RNA interference experimental approach to downregulate NIP7 expression and search for loss-of-function phenotypes. Downregulation of NIP7 in HEK293 cells was efficiently obtained using the transposon-based delivery system described by Heggestad *et al.* (49). Downregulation of NIP7 in HEK293, MCF10A and HeLa cells leads to reduction of cell proliferation rates, with cells accumulating in the G1 phase, indicating that NIP7 plays an important role in all human cells. Downregulation of NIP7 in HEK293 cells affected the levels of 40S ribosomal subunits and caused alterations in pre-rRNA processing which affected mainly the levels of the 34S, 26S and 21S pre-rRNA intermediates. Reduction of the 34S pre-rRNA indicates a slow processing defect at sites 2b and 2c. The increase of the 26S pre-rRNA concentration also correlates with slow processing of site 1 and of sites 2/2b whereas the increase of the 21S pre-rRNA indicates slow processing at sites 2/2b. Primer extension analysis of sites 1, 2b and 3 further supports the northern blot data. At least part of the pre-rRNA processing defects caused by NIP7 depletion have been described for other situations in which ribosome biogenesis was impaired, such as treatment with leptomycin B, which inhibits exportin Crm1/Xpo1 and blocks ribosome subunit export from the nucleus, and for knockdown of 40S biogenesis factors (11). The data obtained in this study indicate that human NIP7 is required primarily for processing of the pre-rRNA intermediates leading to the synthesis of the 18S rRNA and 40S subunit. Taking into account the conditional depletion of yeast Nip7p leads to a deficit of 60S subunits and to accumulation of the 27S pre-rRNA (40), during the course of this work, we have tested whether the human and archaeal *NIP7* orthologs could complement a yeast *Δnip7* mutant strain (Supplementary Figure S1). This analysis showed that neither the human nor the archaeal *NIP7* ortholog can complement a yeast *Δnip7* strain. This finding indicates that although the three orthologs bind structured RNA, and the yeast and human NIP7 are involved in pre-rRNA processing, the function of yeast Nip7p is not fully conserved in human cells.

The interactions of human NIP7 with other proteins are consistent with its role in ribosome biosynthesis. The first interaction described was with Nop132 (43), the putative ortholog of the *S. cerevisiae* Nop8p (44). Tests using the yeast two hybrid system and GST pull-down assays detected association of NIP7 with SBDS, indicating that both proteins may be part of a multisubunit complex (47). Subsequently, human NIP7 was found in association with complexes isolated by affinity-tagged purification of the 40S subunit protein RPS19 (45). This protein was already shown to play an essential role in 40S subunit biosynthesis in human cells (23), consistently with the genetic findings that link mutations in the *RPS19* gene to the DBA (25). Orrù and co-workers (45) described 159 proteins that co-purify with GST-RPS19. Although this complex is heterogeneous, it contains structural components of both the 40S and 60S subunits and a large set of proteins already known to function in ribosome synthesis. NIP7 is also found in complexes isolated by affinity-tagged purification of parvulin (Par14), a peptidyl-prolyl *cis–trans* isomerase (PPIase) reported to function in pre-rRNA processing (46). These large complexes are found mostly in the nucleolus, although some components may be found throughout the whole nucleus, consistently with our data describing NIP7 in the nuclear extracts that sediment in sucrose gradients

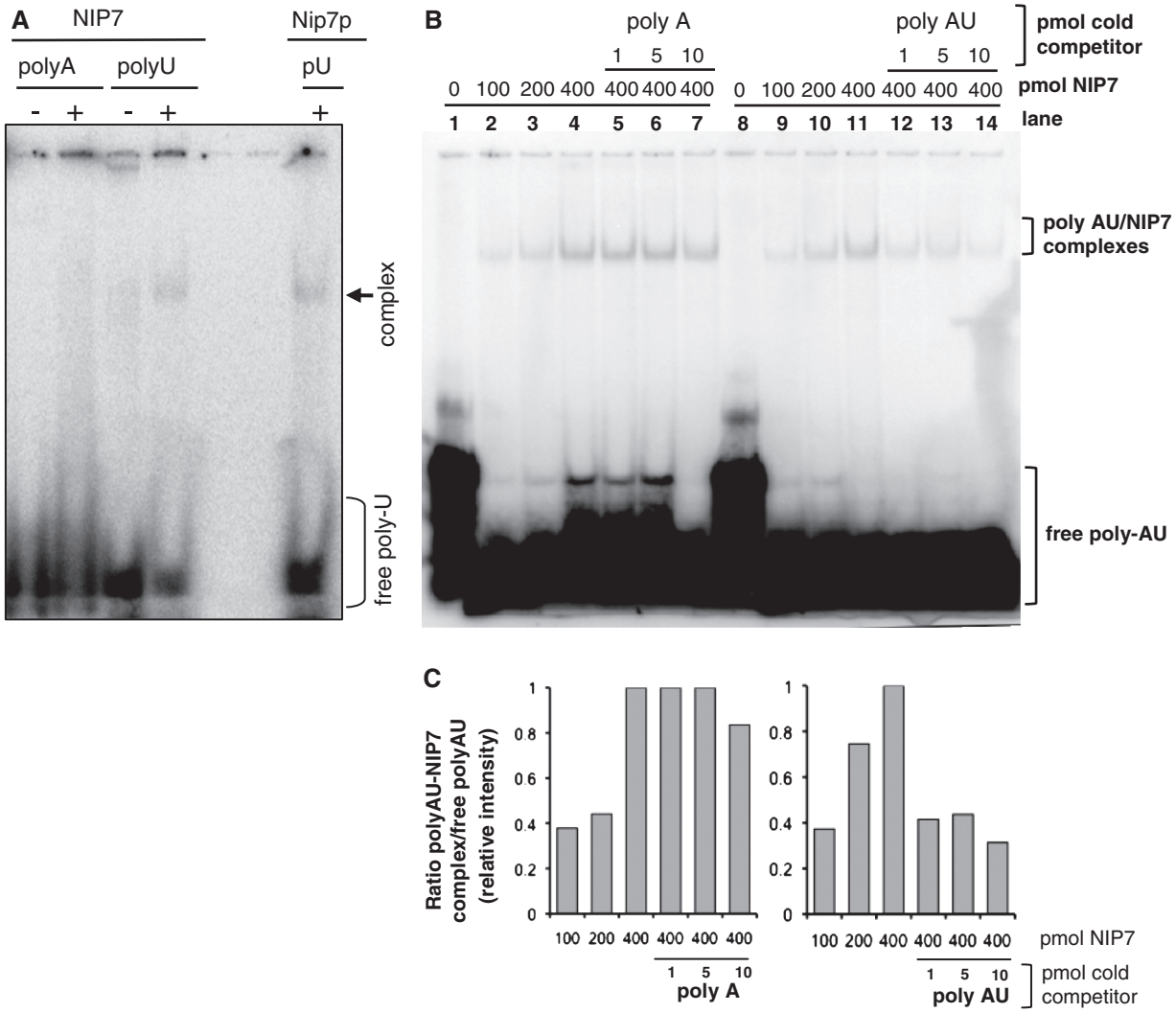

Figure 9. Analysis of NIP7 interaction with RNA *in vitro*. (**A**) Autoradiography of an electrophoretic mobility shift assay to determine the interaction of NIP7 with poly-U. One picomole of [^{32}P]-labeled poly-$A_{(20)}$ (negative control) and poly-$U_{(20)}$ were incubated with 100 pmol of recombinant NIP7. pU indicates the positive control in the assay containing [^{32}P]-labeled poly-$U_{(20)}$ and *S. cerevisiae* Nip7p. The arrow indicates the shifted bands corresponding to the complexes formed by NIP7 and yeast Nip7p with poly-U. (**B**) Autoradiography of an electrophoretic mobility shift assay showing the interaction of NIP7 with poly-AU. A total of 0.4 pmol of a [^{32}P]-labeled 21 mer poly-AU was incubated with 100, 200 and 400 pmol of recombinant NIP7 (lanes 2–4 and 9–11) showing NIP7 concentration dependent complex formation. Parallel competition experiments were performed. In lanes 5–7, 1, 5 and 10 pmol of cold poly-A were used as competitors. No effect of polyA addition is observed on the formation of poly-AU/NIP7 complexes. In lanes 12–14, 1, 5 and 10 pmol of cold poly-AU were used as competitor. As expected, a reduction of poly-AU/NIP7 complex formation is observed. (**C**) Graphs showing the quantitation of the ratio between the amount of polyAU-NIP7 complexes and the amount of free poly-AU of the experiment shown in (B). To calculate the relative intensities, the value of lane 4 was taken as 100% for the binding reactions from lanes 1 to 7 (graph on the left) and the value of lane 11 and taken as 100% for the binding reactions from lanes 8 to 14 (graph on the right).

with molecular masses in the range of 40S–80S ribosomes. During the development of this work, it became clear that the cell extracts used in the sucrose gradient fractionations contained nuclear and nucleolar contaminants probably due to partial leakage of nuclear content during disruption of cells under the hypotonic buffer conditions used or due to partial disruption of nuclei by the 1% v/v Triton detergent that is added to the extraction buffer. Cell fractionation revealed NIP7 only in the nuclear fraction and sucrose gradient fractionation of nuclear extracts indicated that NIP7 co-sediments with high molecular complexes, consistently with its association to pre-ribosomal particles.

Depletion of *S. cerevisiae* Nip7p caused a general defect in pre-rRNA processing, with accumulation of normal (35S and 27S) and of the aberrant (23S) pre-rRNAs and a reduction in the concentration of the mature rRNAs. Despite the global defects on pre-rRNA processing, *S. cerevisiae* Nip7p depletion led to a deficit of 60S subunit (40) and was found in 60S complexes (58). In addition, *S. cerevisiae* Nip7p interacts with a group of proteins involved in ribosome synthesis, including the exosome subunit Rrp43p and the nucleolar proteins Nop8p, Nop53p and Sdo1p (37,44,59,60). These proteins have been implicated to 60S subunit synthesis, although it is important to point out that conditional depletion of the

exosome subunit Rrp43p also led to general defects in pre-rRNA processing resulting in deficit of 40S ribosomal subunits (60). This phenotype is highly unexpected, given that exosome components have previously been reported to be required for excision of the ITS2 segment during maturation of the 3′-end of the 5.8S rRNA, a component of the 60S subunit (61). Further analysis of Rrp43p-depleted cells (60) and of temperature sensitive mutant strains (62) confirmed that deficiency of Rrp43p causes global defects in pre-rRNA processing, making it difficult to distinguish the primary from the secondary defects based only on data obtained from conditional mutants.

Despite the discrepancies between the defects observed in yeast and human NIP7 deficient cells, both human and yeast NIP7 proteins share the ability to bind poly-U *in vitro*, although human NIP7 has shown higher affinity for a poly-AU oligoribonucleotide. NIP7 cognate RNA target sequences have not been identified yet and its preference for binding to poly-U and poly-AU suggests that it might interact with uridine-rich sequences of the pre-rRNA similarly to Rrp5p, which was described to interact with a uridine-rich sequence in the ITS1 of the *S. cerevisiae* pre-rRNA (63). NIP7 orthologs share a two-domain architecture with the C-terminal PUA domain mediating interaction with RNA (42). This domain organization, suggests that NIP7 is an adaptor protein with the C-terminal domain interacting with RNA targets and the N-terminal domain mediating interaction with protein targets.

Saccharomyces cerevisiae NIP7 is part of the Ribi regulon (13,15) and its transcription levels were also shown to correlate with other Ribi regulon genes in response to stress caused by the alkylating agent methyl methanesulfonate (64). In addition, a study based on the analysis of gene expression in response to abrupt changes in environmental conditions has associated *S. cerevisiae* NIP7 to the early repressed ribosomal genes (65). As for the human NIP7 gene, its core promoter contains the 5′-C ACGTG-3′ sequence, also known as E(CG) sequence (66), that is recognized by the Myc:Max heterodimer, indicating that NIP7 is part of the human Ribi regulon proposed to be under control of the Myc transcription factor (16–18).

In conclusion, the data presented in this study show that human NIP7 plays an important role for cell proliferation and implicate NIP7 primarily in the processing of pre-rRNA intermediates leading to maturation of the 18S rRNA and 40S ribosomal subunit biosynthesis. The pre-rRNA processing defects clearly indicate that NIP7 plays a critical role in pre-rRNA processing in human cells. Association of NIP7 to RPS19 complexes (45) helps to explain the pre-RNA processing defects of the 18S rRNA pathway observed in this work for NIP7-depleted cells. We also show evidence that the human NIP7 protein is restricted to the nuclear compartment and that its sedimentation pattern in sucrose gradient fractionation indicates that it is associated to nuclear pre-ribosomal complexes.

SUPPLEMENTARY DATA

Supplementary Data are available at NAR Online.

ACKNOWLEDGEMENTS

The authors are grateful to Carla C. Oliveira for critical reading of the manuscript and discussion during the development of this study. The authors thank Prof. Irene G. H. Lorand-Metze for her support with FACS analyses.

FUNDING

FAPESP (grants CEPID/CBME 98/14138-2 and 06/02083-7) and CNPq (grant 473551/2008-0) to NITZ; FAPESP fellowships (2007/58371-3, 2003/06299-6 and 2006/57653-2 to L.G.M., P.P.C. and C.H.). Funding for open access charge: FAPESP grant Fundação de Amparo à Pesquisa do Estado de São Paulo or from funds from CNPq (Brazilian National Research Council).

Conflict of interest statement. None declared.

REFERENCES

1. Fromont-Racine,M., Senger,B., Saveanu,C. and Fasiolo,F. (2003) Ribosome assembly in eukaryotes. *Gene*, **313**, 17–42.
2. Henras,A., Soudet,K., Gérus,J.M., Lebaron,S., Caizergues-Ferrer,M., Mougin,A. and Henry,Y. (2008) The post-transcriptional steps of eukaryotic ribosome biogenesis. *Cell. Mol. Life Sci.*, **65**, 2334–2359.
3. Peng,W.T., Robinson,M.D., Mnaimneh,S., Krogan,N.J., Cagney,G., Morris,Q., Davierwala,A.P., Grigull,J., Yang,X., Zhang,W. *et al.* (2003) A panoramic view of yeast noncoding RNA processing. *Cell*, **113**, 919–933.
4. Venema,J. and Tollervey,D. (1999) Ribosome synthesis in *Saccharomyces cerevisiae*. *Annu. Rev. Genet.*, **33**, 261–311.
5. Grandi,P., Rybin,V., Bassler,J., Petfalski,E., Strauss,D., Marzioch,M., Schäfer,T., Kuster,B., Tschochner,H., Tollervey,D. *et al.* (2002) 90S pre-ribosomes include the 35S pre-rRNA, the U3 snoRNP, and 40S subunit processing factors but predominantly lack 60S synthesis factors. *Mol. Cell*, **10**, 105–115.
6. Nissan,T.A., Bassler,J., Petfalski,E., Tollervey,D. and Hurt,E. (2002) 60S pre-ribosome formation viewed from assembly in the nucleolus until export to the cytoplasm. *EMBO J.*, **15**, 5539–5547.
7. Tschochner,H. and Hurt,E. (2003) Pre-ribosomes on the road from the nucleolus to the cytoplasm. *Trends Cell Biol.*, **13**, 255–263.
8. Bowman,L.H., Rabin,B. and Schlessinger,D. (1981) Multiple ribosomal RNA cleavage pathways in mammalian cells. *Nucleic Acids Res.*, **9**, 4951–4965.
9. Hadjiolova,K.V., Nicoloso,M., Mazan,S., Hadjiolov,A.A. and Bachellerie,J.-P. (1993) Alternative pre-rRNA processing pathways in human cells and their alteration by cycloheximide inhibition of protein synthesis. *Eur. J. Biochem.*, **212**, 211–215.
10. Kent,T., Lapik,Y.R. and Pestov,D.G. (2009) The 52 external transcribed spacer in mouse ribosomal RNA contains two cleavage sites. *RNA*, **15**, 14–20.
11. Rouquette,J., Choesmel,V. and Gleizes,P.-E. (2005) Nuclear export and cytoplasmic processing of precursors to the 40S ribosomal subunits in mammalian cells. *EMBO J.*, **24**, 2862–2872.
12. Powers,T. and Walter,P. (1999) Regulation of ribosome biogenesis by the rapamycin-sensitive TOR-signaling pathway in *Saccharomyces cerevisiae*. *Mol. Biol. Cell.*, **10**, 987–1000.
13. Gasch,A.P., Spellman,P.T., Kao,C.M., Carmel-Harel,O., Eisen,M.B., Storz,G., Botstein,D. and Brown,P.O. (2000) Genomic expression programs in the response of yeast cells to environmental changes. *Mol. Biol. Cell.*, **11**, 4241–4257.

14. Hannan,K.M., Brandenburger,Y., Jenkins,A., Sharkey,K., Cavanaugh,A., Rothblum,L., Moss,T., Poortinga,G., McArthur,G.A., Pearson,R.B. *et al.* (2003) mTOR-dependent regulation of ribosomal gene transcription requires S6K1 and is mediated by phosphorylation of the carboxy-terminal activation domain of the nucleolar transcription factor UBF. *Mol. Cell. Biol.*, **23**, 8862–8877.
15. Jorgensen,P., Rupeš,I., Sharom,J.R., Schneper,L., Broach,J.R. and Tyers,M. (2004) A dynamic transcriptional network communicates growth potential to ribosome synthesis and critical cell size. *Genes Dev.*, **18**, 2491–2505.
16. Schlosser,I., Hölzel,M., Mürnseer,M., Burtscher,H., Weidle,U.H. and Eick,D. (2003) A role for c-Myc in the regulation of ribosomal RNA processing. *Nucleic Acids Res.*, **31**, 6148–6156.
17. Arabi,A., Wu,S., Ridderstråle,K., Bierhoff,H., Shiue,C., Fatyol,K., Fahlén,S., Hydbring,P., Söderberg,O., Grummt,I. *et al.* (2005) c-Myc associates with ribosomal DNA and activates RNA polymerase I transcription. *Nat. Cell. Biol.*, **7**, 303–310.
18. Grandori,C., Gomez-Roman,N., Felton-Edkins,Z.A., Ngouenet,C., Galloway,D.A., Eisenman,R.N. and White,R.J. (2005) c-Myc binds to human ribosomal DNA and stimulates transcription of rRNA genes by RNA polymerase I. *Nat. Cell. Biol.*, **7**, 311–318.
19. Grewal,S.S., Li,L., Orian,A., Eisenman,R.N. and Edgar,B.A. (2005) Myc-dependent regulation of ribosomal RNA synthesis during Drosophila development. *Nat. Cell. Biol.*, **7**, 295–302.
20. Zhao,Y., Sohn,J.-H. and Warner,J.R. (2003) Autoregulation in the biosynthesis of ribosomes. *Mol. Cell Biol.*, **23**, 699–707.
21. Barna,M., Pusic,A., Zollo,O., Costa,M., Kondrashov,N., Rego,E., Rao,P.H. and Ruggero,D. (2008) Suppression of Myc oncogenic activity by ribosomal protein haploinsufficiency. *Nature*, **456**, 971–975.
22. Dai,M.S. and Lu,H. (2008) Crosstalk between c-Myc and ribosome in ribosomal biogenesis and cancer. *J. Cell. Biochem.*, **105**, 670–677.
23. Choesmel,V., Bacqueville,D., Rouquette,J., Noaillac-Depeyre,J., Fribourg,S., Crétien,A., Leblanc,T., Tchernia,G., da Costa,L. and Gleizes,P.-E. (2007) Impaired ribosome biogenesis in Diamond-Blackfan anemia. *Blood*, **109**, 1275–1283.
24. Cmejla,R., Cmejlova,J., Handrkova,H., Petrak,J. and Pospisilova,D. (2007) Ribosomal protein S17 gene (RPS17) is mutated in Diamond-Blackfan anemia. *Hum. Mutat.*, **28**, 1178–1182.
25. Draptchinskaia,N., Gustavsson,P., Andersson,B., Pettersson,M., Willig,T.N., Dianzani,I., Ball,S., Tchernia,G., Klar,J., Matsson,H. *et al.* (1999) The gene encoding ribosomal protein S19 is mutated in Diamond–Blackfan anaemia. *Nat. Genet.*, **21**, 169–175.
26. Cmejla,R., Cmejlova,J., Handrkova,H., Petrak,J., Petrtylova,K., Mihal,V., Stary,J., Cerna,Z., Jabali,Y. and Pospisilova,D. (2009) Identification of mutations in the ribosomal protein L5 (RPL5) and ribosomal protein L11 (RPL11) genes in Czech patients with Diamond-Blackfan anemia. *Hum. Mutat.*, **30**, 321–327.
27. Farrar,J.E., Nater,M., Caywood,E., McDevitt,M.A., Kowalski,J., Takemoto,C.M., Talbot,C.C. Jr, Meltzer,P., Esposito,D., Beggs,A.H. *et al.* (2008) Abnormalities of the large ribosomal subunit protein, Rpl35a, in Diamond-Blackfan anemia. *Blood*, **11**, 1582–1592.
28. Gazda,H.T., Sheen,M.R., Vlachos,A., Choesmel,V., O'Donohue,M.F., Schneider,H., Darras,N., Hasman,C., Sieff,C.A., Newburger,P.E. *et al.* (2008) Ribosomal protein L5 and L11 mutations are associated with cleft palate and abnormal thumbs in Diamond-Blackfan anemia patients. *Am. J. Hum. Genet.*, **83**, 769–780.
29. Heiss,N.S., Knight,S.W., Vulliamy,T.J., Klauck,S.M., Wiemann,S., Mason,P.J., Poustka,A. and Dokal,I. (1998) X-linked dyskeratosis congenital is caused by mutations in a highly conserved gene with putative nucleolar functions. *Nat. Genet.*, **19**, 32–38.
30. Ruggero,D., Grisendi,S., Piazza,F., Rego,E., Mari,F., Rao,P.H., Cordon-Card,C. and Pandolfi,P.P. (2003) Dyskeratosis congenita and cancer in mice deficient in ribosomal RNA modification. *Science*, **299**, 259–262.
31. Yoon,A., Peng,G., Brandenburger,Y., Zollo,O., Xu,W., Rego,E. and Ruggero,D. (2006) Impaired control of IRES-mediated translation in X-linked dyskeratosis congenital. *Science*, **312**, 902–906.
32. Ridanpaa,M., van Eenennaam,H., Pelin,K., Chadwick,R., Johnson,C., Yuan,B., van Venrooij,W., Pruijn,G., Salmela,R., Rockas,S. *et al.* (2001) Mutations in the RNA component of RNase MRP cause a pleiotropic human disease, cartilage-hair hypoplasia. *Cell*, **104**, 195–203.
33. Gonzales,B., Henning,D., So,R.B., Dixon,J., Dixon,M.J. and Valdez,B.C. (2005) The Treacher Collins syndrome (TCOF1) gene product is involved in pre-rRNA methylation, *Hum. Mol. Genet.*, **14**, 2035–2043.
34. Valdez,B.C., Henning,D., So,R.B., Dixon,J. and Dixon,M.J. (2004) The Treacher Collins syndrome (TCOF1) gene product is involved in ribosomal DNA gene transcription by interacting with upstream binding factor. *Proc. Natl Acad. Sci. USA*, **101**, 10709–10714.
35. Boocock,G.R., Morrison,J.A., Popovic,M., Richards,N., Ellis,L., Durie,P.R. and Rommens,J.M. (2003) Mutations in SBDS are associated with Shwachman–Diamond syndrome. *Nat. Genet.*, **33**, 97–101.
36. Ganapathi,K.A., Austin,K.M., Lee,C.S., Dias,A., Malsch,M.M, Reed,R. and Shimamura,A. (2007) The human Shwachman-Diamond syndrome protein, SBDS, associates with ribosomal RNA. *Blood*, **110**, 1458–1465.
37. Luz,J.S., Georg,R.C., Gomes,C.H., Machado-Santelli,G.M. and Oliveira,C.C. (2009) Sdo1p, the yeast ortholog of Shwachman-Bodian-Diamond syndrome protein binds RNA and interacts with nuclear rRNA processing factors. *Yeast*, **26**, 287–298.
38. Menne,T.F., Goyenechea,B., Sánchez-Puig,N., Wong,C.C., Tonkin,L.M., Ancliff,P.J., Brost,R.L., Costanzo,M., Boone,C. and Warren,A.J. (2007) The Shwachman-Bodian-Diamond syndrome protein mediates translational activation of ribosomes in yeast. *Nat. Genet.*, **39**, 486–495.
39. Belin,S., Beghin,A., Solano-Gonzàlez,E., Bezin,L., Brunet-Manquat,S., Textoris,J., Prats,A.C., Mertani,H.C., Dumontet,C. and Diaz,J.-J. (2009) Dysregulation of ribosome biogenesis and translational capacity is associated with tumor progression of human breast cancer cells. *PLoS ONE*, **4**, e7147.
40. Zanchin,N.I.T., Roberts,P., de Silva,A., Sherman,F. and Goldfarb,D.S. (1997) *Saccharomyces cerevisiae* Nip7p is required for efficient 60S ribosome subunit biogenesis. *Mol. Cell. Biol.*, **17**, 5001–5015.
41. Aravind,L. and Koonin,E. (1999) Novel predicted RNA-binding domains associated with the translation machinery. *J. Mol. Biol.*, **48**, 291–302.
42. Coltri,P.P., Guimarães,B.G., Granato,D.C., Luz,J.S., Teixeira,E., Oliveira,C.C. and Zanchin,N.I.T. (2007) Structural insights into the interaction of the Nip7 PUA domain with polyuridine RNA. *Biochemistry*, **46**, 14177–14187.
43. Sekiguchi,T., Todaka,Y., Wang,Y., Hirose,E., Nakashima,N. and Nishimoto,T. (2004) A novel human nucleolar protein, Nop132, binds to the G proteins, RRAG A/C/D. *J. Biol. Chem.*, **279**, 8343–8350.
44. Zanchin,N.I.T. and Goldfarb,D.S. (1999) Nip7p interacts with Nop8p, an essential nucleolar protein required for 60S ribosome biogenesis, and the exosome subunit Rrp43p. *Mol. Cell. Biol.*, **19**, 1518–1525.
45. Orrù,S., Aspesi,A., Armiraglio,M., Caterino,M., Loreni,F., Ruoppolo,M., Santoro,C. and Dianzani,I. (2007) Analysis of the ribosomal protein S19 interactome. *Mol. Cell. Proteomics*, **6**, 382–393.
46. Fujiyama-Nakamura,S., Yoshikawa,H., Homma,K., Hayano,T., Tsujimura-Takahashi,T., Izumikawa,K., Ishikawa,H., Miyazawa,N., Yanagida,M., Miura,Y. *et al.* (2009) Parvulin (Par14), a peptidyl-prolyl cis-trans isomerase, is a novel rRNA processing factor that evolved in the metazoan lineage. *Mol. Cell. Proteomics*, **8**, 1552–1565.
47. Hesling,C., Oliveira,C.C., Castilho,B.A. and Zanchin,N.I.T. (2007) The Shwachman-Bodian-Diamond syndrome associated protein interacts with HsNip7 and its down-regulation affects gene expression at the transcriptional and translational levels. *Exp. Cell Res.*, **313**, 4180–4195.
48. Sambrook,J., Fritsch,E.J. and Maniatis,T. (1989) *Molecular cloning, A Laboratory Manual*, 2nd edn. Cold Spring Harbor Laboratory Press, Cold Spring Harbor, NY.

49. Heggestad,A.D., Notterpek,L. and Fletcher,B.S. (2004) Transposon based RNAi delivery system for generating knockdown cell lines. *Biochem. Biophys. Res. Commun.*, **316**, 643–650.
50. Klan,N. and Steinhilber,D. (2003) Transient transfection of the human myeloid cell line Mono Mac 6 using electroporation. *Biotechniques*, **34**, 142–147.
51. Johannes,G. and Sarnow,P. (1998) Cap-independent polysomal association of natural mRNAs encoding c-myc, BiP, and eIF4G conferred by internal ribosome entry sites. *RNA*, **12**, 1500–1513.
52. Gonzales,F.A., Zanchin,N.I.T., Luz,J.S. and Oliveira,C.C. (2005) Characterization of *Saccharomyces cerevisiae* Nop17p, a novel Nop58p-interacting protein that is involved in pre-rRNA processing. *J. Mol. Biol.*, **346**, 437–455.
53. Lebreton,A., Tomecki,R., Dziembowski,A. and Séraphin,B. (2008) Endonucleolytic RNA cleavage by a eukaryotic exosome. *Nature*, **456**, 993–996.
54. Bowman,L.H., Goldman,W.E., Goldberg,G.I., Herbert,M.B. and Schiessinger,D. (1983) Location of the initial cleavage sites in mouse pre-rRNA. *Mol. Cell. Biol.*, **3**, 1501–1510.
55. Rubin,G.M. (1974) Three forms of the 5.8S ribosomal RNA species in *Saccharomyces cerevisiae*. *Eur. J. Biochem.*, **41**, 197–202.
56. Smith,S.D., Banerjee,N. and Sitz,T.O. (1984) Gene heterogeneity: a basis for alternative 5.8S rRNA processing. *Biochemistry*, **23**, 3648–3652.
57. Schmitt,M.E. and Clayton,D.A. (1993) Nuclear RNase MRP is required for correct processing of pre-5.8S rRNA in *Saccharomyces cerevisiae*. *Mol. Cell. Biol.*, **13**, 7935–7941.
58. Lebreton,A., Rousselle,J.-C., Lenormand,P., Namane,A., Jacquier,A., Fromont-Racine,M. and Saveanu,C. (2008) 60S ribosomal subunit assembly dynamics defined by semi-quantitative mass spectrometry of purified complexes. *Nucleic Acids Res.*, **36**, 4988–4999.
59. Granato,D.C., Gonzales,F.A., Luz,J.S., Cassiola,F., Machado-Santelli,G.M. and Oliveira,C.C. (2005) Nop53p, an essential nucleolar protein that interacts with Nop17p and Nip7p, is required for pre-rRNA processing in *Saccharomyces cerevisiae*. *FEBS J.*, **272**, 4450–4463.
60. Zanchin,N.I.T. and Goldfarb,D.S. (1999) The exosome subunit Rrp43p is required for the efficient maturation of 5.8S, 18S and 25S rRNA. *Nucleic Acids Res.*, **27**, 1283–1288.
61. Mitchell,P., Petfalski,E., Shevchenko,S., Mann,M. and Tollervey,D. (1997) The exosome: a conserved eukaryotic RNA processing complex containing multiple 3′-5′ exoribonucleases. *Cell*, **91**, 457–466.
62. Oliveira,C.C., Gonzales,F.A. and Zanchin,N.I.T. (2002) Temperature-sensitive mutants of the exosome subunit Rrp43p show a deficiency in mRNA degradation and no longer interact with the exosome. *Nucleic Acids Res.*, **30**, 4186–4198.
63. de Boer,P., Vos,H.R., Faber,A.W., Vos,J.C. and Raué,H.A. (2006) Rrp5p, a trans-acting factor in yeast ribosome biogenesis, is an RNA-binding protein with a pronounced preference for U-rich sequences. *RNA*, **12**, 263–271.
64. Jelinsky,S.A. and Samson,L.D. (1999) Global response of *Saccharomyces cerevisiae* to an alkylating agent. *Proc. Natl Acad. Sci. USA*, **96**, 1486–1491.
65. Chechik,G. and Koller,D. (2009) Timing of gene expression responses to environmental changes. *J. Comput. Biol.*, **16**, 279–290.
66. Brown,S.J., Cole,M.D. and Erives,A.J. (2008) Evolution of the holozoan ribosome biogenesis regulon. *BMC Genomics*, **9**, 442, doi:10.1186/1471-2164-9-442.